universität wien

MASTERARBEIT / MASTER'S THESIS

Titel der Masterarbeit / Title of the Master's Thesis

„Generation of molecular tools for the analysis of Dishevelled and Hox/Gbx function in the sea anemone *Nematostella vectensis*"

verfasst von / submitted by

Thomas Eckhardt, Bsc

angestrebter akademischer Grad / in partial fulfilment of the requirements for the degree of

Master of Science (MSc)

Wien, 2023 / Vienna, 2023

Studienkennzahl lt. Studienblatt / degree programme code as it appears on the student record sheet:	UA 066 831
Studienrichtung lt. Studienblatt / degree programme as it appears on the student record sheet:	Masterstudium Zoologie
Betreut von / Supervisor:	Mag. Dr. Grigory Genikhovich, Privatdoz.
Mitbetreut von / Co-Supervisor:	

Acknowledgements

First and foremost, I would like to express my sincere gratitude to Grigory Genikhovich for giving me the opportunity to work on this project. I cannot stress enough how much I value the time you took to answer each and every one of my questions. Moreover, I would like to thank David Mörsdorf, Paul Knabl, Tatiana Lebedeva, and Sanjay Narayanaswamy for their support and valuable input and Angela Caballero Alfonso for keeping the *Nematostella* facility running.

Table of Contents

Abstract

In most animals, early development is driven by maternally deposited as well as zygotically produced regulatory molecules. Deciphering the embryonic function of these molecules and, consequently, the evolution of the associated developmental mechanisms hinges on the ability to manipulate them effectively. This, in turn, requires the appropriate molecular tools. Here, I focus on developing the means to address two key developmental mechanisms in the sea anemone *Nematostella vectensis*: endoderm specification and axis patterning. First, I generate the molecular tools that will allow studying the role of maternally deposited proteins like Dishevelled in endoderm specification. Traditionally, protein function is disrupted either at the mRNA or genome level. However, these indirect approaches do not target proteins already present in the egg at the time of fertilisation. To achieve that, I developed a novel molecular tool based on the E3 ubiquitin ligase adapter protein SPOP fused to an αGFP or αmCherry nanobody. This offers the opportunity to directly degrade previously inaccessible maternally deposited proteins if tagged with one of these fluorescent proteins. Additionally, I set out to investigate the functional interplay between *Hox* genes and *Gbx* responsible for patterning the directive axis. They exhibit a regulatory behaviour strikingly reminiscent of the posterior prevalence phenomenon seen in bilaterians. To study the underlying mechanism, I used CRISPR/Cas9-mediated gene knock-in. I identified working gRNAs by qPCR melt curve analysis and successfully tagged *HoxDa* with *mCherry*. With this, I lay the groundwork for future research on the early embryogenesis of *Nematostella*.

Zusammenfassung

Die frühe Entwicklung vieler Tiere wird von maternal platzierten sowie zygotisch produzierten regulatorischen Molekülen bestimmt. Diese effektiv manipulieren zu können, ist eine Voraussetzung, um ihre embryonale Funktion und folglich die Evolution der damit verbundenen Entwicklungsmechanismen zu entschlüsseln. Dafür notwendig, sind die geeigneten molekularen Werkzeuge. Hier beschäftige ich mich damit die Mittel zur Untersuchung von zwei wichtigen Entwicklungsmechanismen in der Seeanemone *Nematostella vectensis* herzustellen: der Spezifikation des Endoderms sowie der Musterung der Körperachse. Zuerst stelle ich die molekularen Werkzeuge her, die es zukünftig ermöglichen werden, die Rolle von maternal platzierten Proteinen wie Dishevelled bei der Spezifikation des Endoderms zu untersuchen. Traditionell wird die Proteinfunktion entweder auf der mRNA- oder der Genomebene manipuliert. Diese indirekten Ansätze zielen jedoch nicht auf Proteine ab, die bereits vor der Befruchtung im Ei vorhanden sind. Diesbezüglich habe ich ein neues Werkzeug - basierend auf dem E3-Ubiquitin-Ligase-Adapterprotein SPOP fusionierend mit einem αGFP- oder αmCherry-Nanokörper - entwickelt. Es bietet die Möglichkeit, bisher unzugängliche maternale Proteine direkt abzubauen, wenn sie mit einem dieser beiden fluoreszierenden Proteine markiert sind. Außerdem wollte ich das funktionelle Zusammenspiel zwischen *Hox* Genen und *Gbx* untersuchen, die für die Musterung der direktiven Achse verantwortlich sind. Sie zeigen ein regulatorisches Verhalten, welches an das Phänomen der „posterioren Prävalenz“ bei Bilateria erinnert. Um den zugrunde liegenden Mechanismus zu analysieren, habe ich die CRISPR/Cas9 Technologie eingesetzt. Ich identifizierte zunächst funktionierende gRNAs durch qPCR-Schmelzkurvenanalyse und knockte anschließend *mCherry* in den endogenen *HoxDa*-locus. Mit dieser Arbeit lege ich den Grundstein für zukünftige Untersuchungen zur frühen Embryogenese von *Nematostella*.

1. Introduction

Oocytes of many metazoan species are teeming with maternally deposited transcripts and proteins, unevenly distributed along the animal-vegetal axis (Lee et al., 2014). They orchestrate early embryogenesis, determining key developmental processes like gastrulation. As development proceeds, control is handed over to the zygotic genome, and a conserved toolkit of signalling pathways and transcription factors patterns the body axes and drives the remaining developmental program (De Robertis, 2008; Genikhovich and Technau, 2017; Niehrs, 2010). Thus, embryonic development relies on maternally deposited (in short: maternal) as well as zygotically produced regulatory molecules. The ability to manipulate these molecules is crucial for understanding their embryogenetic function and, consequently, for deciphering the evolution of developmental mechanisms. Here, I focus on two such mechanisms in the sea anemone *Nematostella vectensis.* I set out to generate the molecular tools that will enable studying (i) the role of maternally deposited proteins such as Dishevelled in endoderm specification and (ii) the functional interplay between *Hox* genes and *Gbx* responsible for patterning the directive axis.

The endomesoderm in bilaterians is specified by a β-catenin signal at the vegetal pole of the embryo (Darras et al., 2011; Henry et al., 2008; Logan et al., 1999; McClay et al., 2021). In *Nematostella* blastula, maternal β-catenin likewise accumulates at one side. When β-catenin is downregulated, the embryo fails to gastrulate and remains a blastula-like sphere (Leclère et al., 2016; Wikramanayake et al., 2003). This implied that an early β-catenin signal similarly regulates endoderm specification in *Nematostella*. Contrary to bilaterians, however, it was assumed that β-catenin is localised at the animal pole, as this is where cnidarians with a unipolar mode of gastrulation internalise their endoderm (Fritzenwanker et al., 2007). This assumption was further supported by the detection of the maternal Dishevelled protein at the animal pole (Lee et al., 2007). Dishevelled plays a key role in the Wnt/β-catenin pathway. When Wnt ligands bind to Frizzled receptors, Dishevelled is recruited to the cell membrane, where it inhibits the APC, Axin, CK1-α, and GSK-3β-mediated degradation of β-catenin, enabling β-catenin to translocate into the nucleus (Sharma et al., 2018). In sea urchins, maternal Dishevelled protein co-localizes with β-catenin at the vegetal pole (Fig. 1.) In *Nematostella*, it is said to accumulate at the animal pole of the oocyte and the cortex of the animal pole blastomeres, which corresponds to the then presumed β-catenin-positive side (Kumburegama and Wikramanayake, 2007; Lee et al., 2007).

Several observations, however, challenged the view that β-catenin specifies the endoderm in *Nematostella*. For example, while β-catenin morphants do not gastrulate and remain a blastula-like sphere, they ubiquitously express the endodermal marker *SnailA* rather than the anterior ectoderm markers, as it would be the case in bilaterians. Overexpressing β-catenin, on the other hand, leads to the same spherical phenotype, but in this case, oral ectodermal markers such as *Brachyury*, *FoxA,* and *FoxB* are expressed, while the endodermal markers are completely abolished (Lebedeva et al., 2021; Leclère et al., 2016). These results indicated that β-catenin represses rather than activates endoderm specification in *Nematostella*. Ultimately, a knock-in line in which endogenous β-catenin was fused in-frame with sfGFP revealed that early nuclear β-catenin accumulates not at the animal pole, as expected, but, surprisingly, at the vegetal pole, i.e., opposite of the gastrulation side (Lebedeva et al., 2022). Taken together, maternal β-catenin in *Nematostella,* as in various bilaterians, accumulates at the vegetal pole. However, unlike in bilaterians, it does not activate endoderm specification but instead represses it, resulting in gastrulation occurring at the β-catenin-negative animal pole (Fig.1). This, in turn, prompts the question: if, as indicated, maternal β-catenin and Dishevelled do not co-localise at the same pole but instead accumulate on opposite poles, what then is the function of maternal Dishevelled protein during the early embryogenesis of *Nematostella*? To address this, one first needs to re-evaluate the localisation of Dishevelled. For this purpose, a knock-in line in which endogenous Dishevelled is tagged in-frame with mCherry is currently being generated. This line will then further be used to study the function of maternal Dishevelled. To do so, I am establishing a novel molecular tool that enables the targeted degradation of fusion proteins.

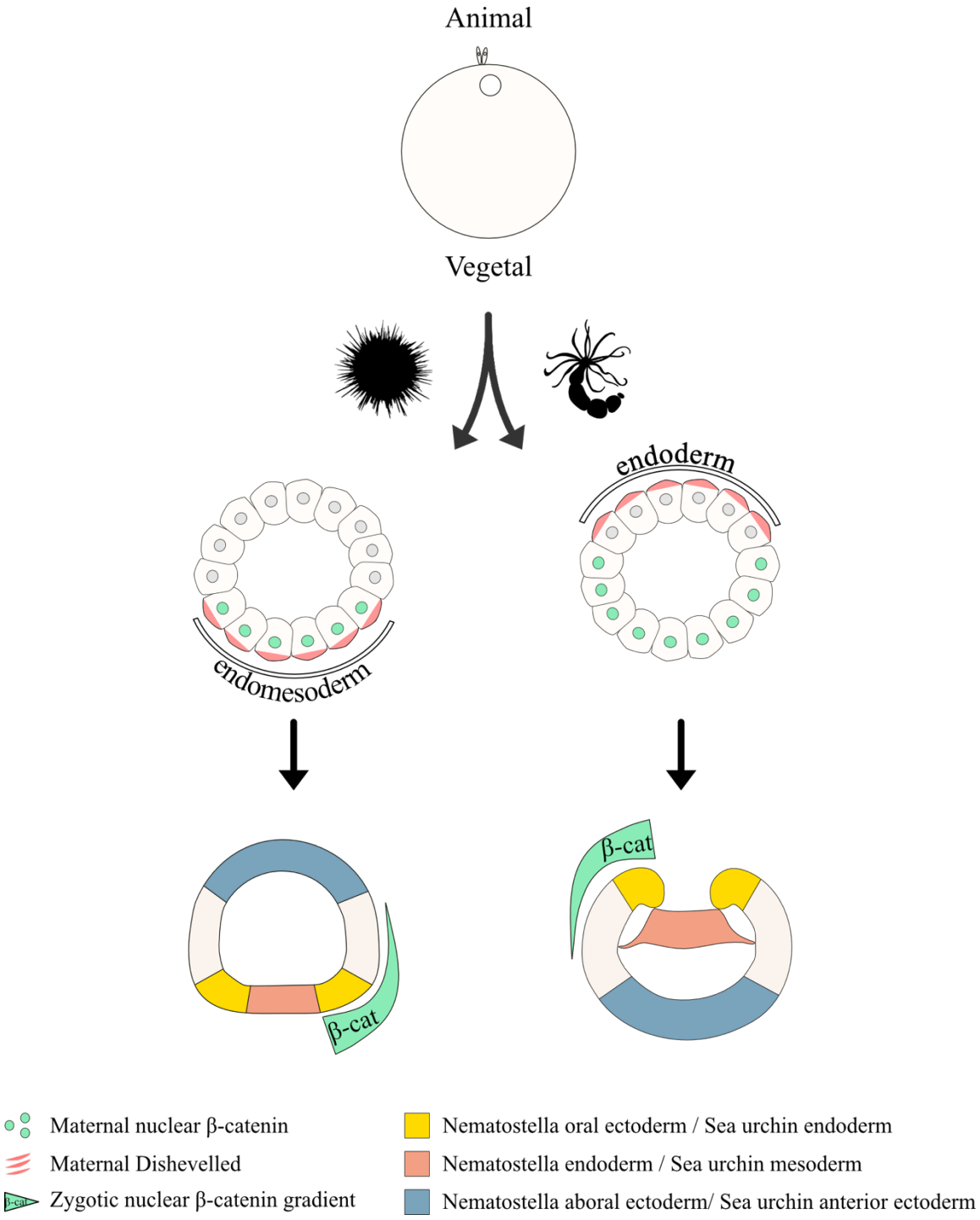

Fig. 1. Maternal Dishevelled protein and maternal nuclear β-catenin co-localise in sea urchin but accumulate at opposing poles in *Nematostella*. In *Nematostella* and sea urchin, maternal β-catenin accumulates at the vegetal pole nuclei. In *Nematostella*, however, the endoderm is specified at the β-catenin negative animal pole. A zygotic β-catenin gradient patterns the oral-aboral axis. Animal pictograms are from https://www.phylopic.org/. The figure is modified after Lebedeva et al., 2022.

The animal-vegetal axis of the oocyte corresponds to the future oral–aboral axis. Orthogonal to it, anthozoan cnidarians like *Nematostella* exhibit an additional secondary body axis. This "directive" axis is set in the gastrula and patterned in the planula larvae by *Hox* genes and *Gbx*

under the direct control of Bone Morphogenetic Protein (BMP) signalling (Genikhovich et al., 2015; He et al., 2018; Knabl et al., 2022). In Bilateria, *Hox* genes encode transcription factors and are frequently expressed in staggered, partially overlapping domains along the anterior-posterior body axis. This arrangement provides each region along the axis with a unique "*Hox* code" and specifies it accordingly (Akam, 1998; Hunt and Krumlauf, 1992). All *Hox* genes have a very precise **a**nterior **e**xpression **b**oundary (AEB). Interestingly, *Hox* genes with a more posteriorly located AEB functionally override the overlapping *Hox* genes with a more anteriorly located AEB (Fig.1). This phenomenon is known as "posterior prevalence". It is showcased by the homeotic transformation of, e.g., the haltere-bearing third thoracic segment into a duplicated wing-bearing second thoracic segment in a *Ubx*$^{-/-}$ *Drosophila* (Diaz-de-la-Loza et al., 2020) or lumbar vertebrae into rib-bearing thoracic vertebrae in a *HoxPG10*$^{-/-}$ mouse (Mallo et al., 2010; Wellik and Capecchi, 2003). In both examples, due to the loss of the more posteriorly expressed *Hox* gene (*HoxPost*), a *Hox* gene with a partially overlapping expression but a more anterior AEB (*HoxAnt*) re-specifies the identity of the segments located posteriorly to the domain that is normally defined by *HoxAnt* (Fig.2*).* The underlying regulatory mechanisms are not fully understood.

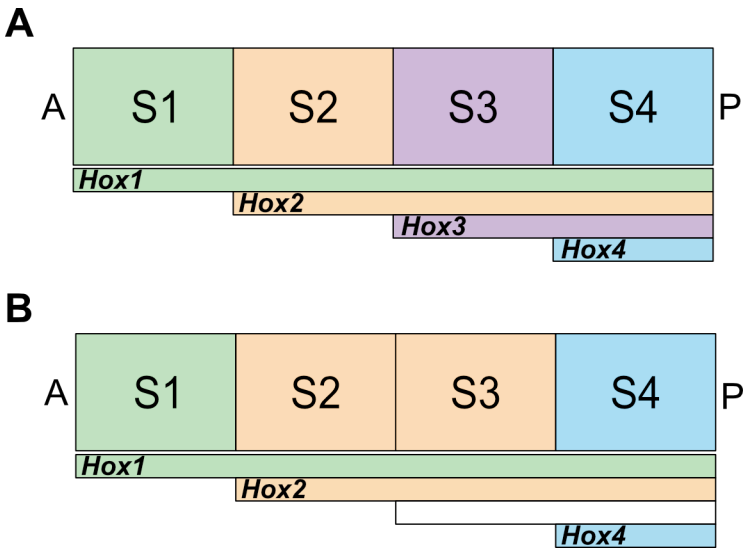

Fig.2 Schematic representation of *Hox* gene "posterior prevalence". (A) *Hox* genes with a more posteriorly located anterior expression boundary (AEB) functionally override the overlapping *Hox* genes with a more anteriorly located AEB. *Hox4* functionally overrides *Hox3, Hox2,* and *Hox1* in S4 and specifies the identity of S4. *Hox3* overrides *Hox2* and *Hox1* in S3 and specifies S3. *Hox2* overrides *Hox1* in S2 and specifies S2. *Hox1* specifies S1. **(B)** Example of the change of segment identity upon loss of a *Hox* gene. Loss of *Hox3* results in S3 being specified by *Hox2.* Since S2 and S3 are both specified by *Hox2,* they have the same segment identity. A = anterior, P = posterior, S = segment, Coloured bars = expression domains of different *Hox* genes.

Three *Hox* genes, *HoxE*, *HoxDa*, *HoxB*, and the non-Hox Antennapedia class homeobox gene *Gbx*, pattern the directive axis of *Nematostella*. They, too, are expressed in staggered, partially overlapping domains (He et al., 2018). Moreover, their expression boundaries

precisely correspond to the boundaries of the eight emerging mesenterial segments. These segments can be subdivided into three paired segments - S2/S8, S3/7, S4/S6 - and the two unpaired segments, S5 and S1, positioned at the strong and weak BMP signalling end of the axis, respectively. As in bilaterians, the arrangement of these *Hox* genes and *Gbx* provides each segment or segment pair with a unique *Hox/Gbx* code. Changing the *Hox/Gbx* code by knocking down or knocking out any of the four genes changes the developmental fate of specific segments and the formation of segment boundaries. This regulatory behaviour is strikingly reminiscent of posterior prevalence, i.e., each *Hox* gene with an expression boundary closer to the strong BMP signalling end of the axis (S5) functionally inhibits the other *Hox*/*Gbx* genes, even though they are co-expressed at the mRNA level (Fig.3) (He et al., 2018). This raises the question: how and at what level is the functional interplay between *Hox* genes and *Gbx* genes regulated in *Nematostella*?

I propose two hypothetical explanations (Fig.3). First, the Hox/Gbx protein responsible for the fate of a segment might inhibit the translation of the other *Hox* and *Gbx* transcripts in that given segment. For example, *HoxDa* is expressed in the S4/S6 pair, which it specifies, and in S5, which is specified by HoxE. According to this hypothesis, HoxDa protein inhibits the translation of *HoxB* and *Gbx* transcripts in S4/S6, while its own translation is inhibited by HoxE protein in S5. Therefore, the HoxDa protein would only be present in S4/S6. Alternatively, the Hox/Gbx protein responsible for the fate of a segment might outcompete the other Hox and Gbx proteins when binding to the binding sites in the enhancers of their shared target genes (Crocker et al., 2015). In the same example, HoxDa outcompetes HoxB and Gbx in S4/6 but, in turn, is outcompeted by HoxE in S5. In this case, however, transcripts and their respective proteins would co-localize. To test these two hypotheses, fluorescently tagged versions of all the Hox/Gbx proteins need to be generated. Direct observation of fluorescence will allow evaluation of the translational inhibition hypothesis, and ChIP-Seq with antibodies against the tag will show whether different *Hox* genes and *Gbx* genes share transcriptional targets and, possibly, compete for them. To achieve that, I use CRISPR/Cas9-mediated gene knock-in and, after having identified working guide RNAs, set out to tag *HoxDa*, *HoxB*, and *Gbx* with coding sequences of different reporters.

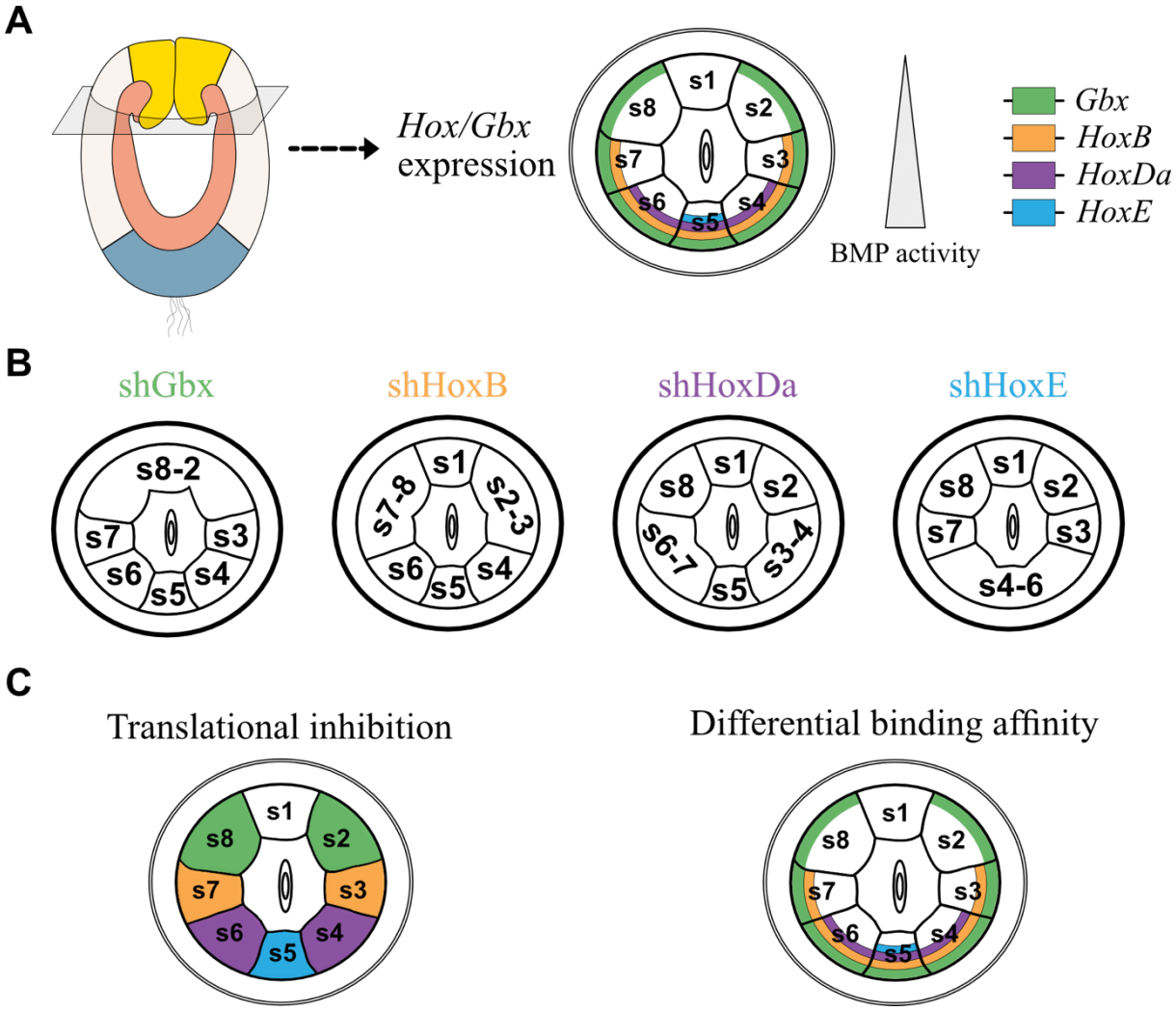

Fig. 3. *Hox* genes and *Gbx* genes specify the segments along the directive axis following a "posterior prevalence" regulatory behaviour. (A) *Hox* genes and *Gbx*, under the control of BMP signalling, specify the regions along the directive axis in the planula larva. **(B)** shRNA-mediated phenotypes showcase the regulatory behaviour between the *Hox/Gbx* genes. Knockdown of any of the four genes abolishes the mesentery at its expression boundary positioned towards the weak BMP signalling end (S1), resulting in the fusion and homeotic transformation of the involved segments. **(C)** The mechanism governing the functional interplay between *HoxE, HoxDa, HoxB,* and *Gbx* is unclear. Two explanations are proposed. The "translational inhibition" hypothesis states that a segment's dominant Hox transcription factor inhibits translation of the other *Hox*/*Gbx* transcripts in that segment. The "differential binding affinity" hypothesis states that the dominant Hox protein in a segment outcompetes the other Hox/Gbx proteins when binding to the binding sites in the enhancers of their target genes. Putative protein localisation differs in the two scenarios. The figure is modified after He et al., 2018.

Here, I demonstrate a novel molecular tool – the BTB protein SPOP fused to an αGFP or αmCherry nanobody - that enables the targeted degradation of fusion proteins. I show that both αGFP-SPOP and αmCH-SPOP are functional, providing the opportunity to manipulate

and thereby deduce the function of previously inaccessible maternal proteins in *Nematostella*. Furthermore, I use CRISPR/Cas9 mediated gene knock-in to tag HoxDa, HoxB, and Gbx with different reporters. For that purpose, I identify working guide RNAs using qPCR melt curve analysis and then successfully knock-in *mCherry* at the C-terminus of *HoxDa*.

2. Results

2.1 Establishing a molecular tool for targeted protein degradation

2.1.1 Utilising the ubiquitin-proteasome system

There are two common approaches for interfering with the function of a protein. At the genome level, methods such as CRISPR/Cas9 genome editing allow precise modifications of a gene coding for a protein of interest (Doudna and Charpentier, 2014). By creating insertions or deletions, the reading frame of the gene can be disrupted, leading to a non-functional protein. Alternatively, at the RNA level, methods such as morpholinos or RNAi are employed (Fire et al., 1998; Heasman, 2002). They either block or degrade the mRNA, leading to the corresponding protein not being translated. In both approaches, however, protein function is disrupted indirectly. Proteins that are already present in the cells at the time of the abovementioned manipulations are not targeted. For this purpose, I developed a tool that enables targeted protein degradation by utilising the ubiquitin-proteasome system (UPS). It is based on a similar tool established in Zebrafish (Ju Shin et al., 2015). The UPS is a major regulatory mechanism in eukaryotic cells (Chondrogianni and Gonos, 2012; Ciechanover, 2015; Glickman and Ciechanover, 2002). It coordinates intracellular protein degradation via a cascade reaction that ultimately attaches ubiquitin to the lysine residues of substrate proteins, marking them for downstream regulatory interactions such as proteolysis. Three enzymes catalyse ubiquitination: E1 ubiquitin-activating enzyme, E2 ubiquitin-conjugating enzyme, and E3 ubiquitin ligase (Li et al., 2022) (Fig.4.) E3s either directly or indirectly transfer ubiquitin from the E2 enzyme to the substrate protein (Chondrogianni and Gonos, 2012). Therefore, they confer specificity to the ubiquitination system, making them the key unit of the UPS to utilise as a tool for targeted protein degradation.

2.1.2 A modified BTP protein acts as a tool for the targeted degradation of fusion proteins

As a framework for the degradation tool, I used a subfamily of the highly diverse Cullin-RING E3 ligases (CRLs) known as Cullin3-RING ubiquitin ligases (CRL3s) (Genschik et al., 2013). Structurally, they share similar core modules as other CRLs: a substrate recognition

module that interacts with the target protein, a RING-box protein that binds to E2, and a Cullin protein that acts as a scaffold between the two (Petroski and Deshaies, 2005). However, whereas the substrate recognition module of other CRLs consists of a separate substrate receptor protein and a Cullin binding adaptor protein forming a heterodimer, CRL3s combine these two functions in a single-unit Bric-`a-brac/Tramtrack/Broad (BTB) protein (Genschik et al., 2013; Li et al., 2022). Taking advantage of this dual function of BTBs, I replaced the substrate binding domain of the *Nematostella* Speckle Type BTB/POZ Protein (SPOP) with an αGFP or αmCherry nanobody while leaving the Cullin binding adaptor domain intact. The nanobody-SPOP fusion protein should bind explicitly to proteins containing either GFP or mCherry and, through its adaptor domain, recruit them to Cullin3, where they will be ubiquitinated and subsequently degraded by the proteasome.

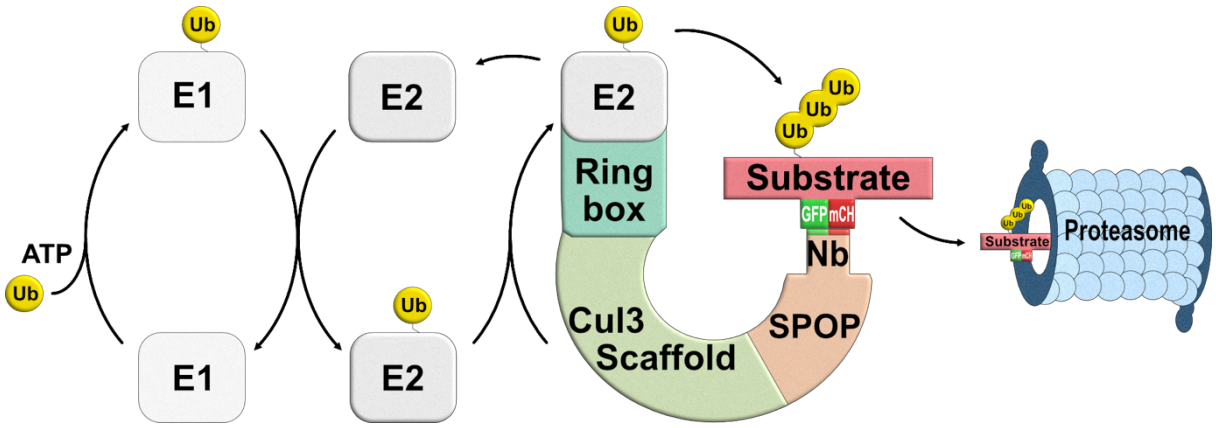

Fig. 4. UPS-mediated proteolysis of mCherry- or GFP-tagged fusion proteins. Targeted proteins are ubiquitinated via an enzymatic cascade involving an E1 ubiquitin-activating enzyme, an E2 ubiquitin-conjugating enzyme, and a synthetic Cullin3-RING ubiquitin ligase in which the substrate binding domain of the BTB protein SPOP is replaced by an αmCherry or αGFP nanobody. The ubiquitin-labeled substrate is recognised and degraded by the proteasome. Ub = Ubiquitin, Nb = αmCherry or αGFP nanobody.

2.1.3 The sfGFP-β-catenin line is the optimal system for testing the Nb-SPOP tool

To test whether Nb-SPOP could effectively degrade maternally deposited proteins, I required a system with tagged proteins which are detectable in the oocyte and zygote and a predictable phenotype upon manipulation of these proteins. Both conditions are met by the *sfGFP-β-catenin* transgenic line (Lebedeva et al., 2022). Tagged *β-catenin* is maternally deposited in the oocyte as protein and mRNA (Lebedeva et al., 2022). This offers a key advantage. The degradation tool will also inevitably target the β-catenin protein translated from maternal

mRNA. Since morpholinos have been used to block the translation of maternal *β-catenin* mRNA, there is a known phenotype upon partial knockdown of the maternal β-catenin signal (Leclère et al., 2016). It can act as a benchmark for the functionality of Nb-SPOP. Moreover, the role of zygotic Wnt/β-catenin signalling for patterning the ectoderm along the oral-aboral axis has been addressed in detail (Leclère et al., 2016; Niedermoser et al., 2022). This will allow me to determine whether Nb-SPOP is functional early enough to target the maternal β-catenin signal or if only zygotic β-catenin is affected.

2.1.4 *αGFP*-SPOP is functional and specific

Having identified the right system, I first tested whether the fluorescence signal of *sfGFP-β-catenin* F3 zygotes is visibly reduced upon injection of *αGFP-SPOP or* αGFP-SPOPΔNLS mRNA. The latter was tested because deletion of the C-terminal nuclear localisation signal (NLS) of SPOP was shown to enhance its degradation efficacy in a similar tool used on Zebrafish (Wang et al., 2022). I measured the fluorescent intensity of both groups at 24 hpf and 48 hpf and compared it to that of *sfGFP-β-catenin* embryos that were either uninjected or injected with *αmCherry-SPOP* mRNA (Fig. 5 and Fig. S1). Whereas both control groups showed a strong ubiquitous GFP signal, the fluorescence intensity of αGFP-SPOP injected embryos (both with and without NLS) was decreased by about 50 %. This provided an initial indication that αGFP-SPOP successfully targets sfGFP-β-catenin. Since deleting the NLS did not enhance degradation efficacy, I focused on using *αGFP-SPOP* and disregarded *αGFP-SPOPΔNLS* from here on. To next assess whether the decrease of fluorescent intensity is indeed a result of sfGFP-β-catenin degradation, I performed a western blot on protein extracts of αGFP-SPOP injected embryos and the same control groups as above plus uninjected wildtypes (Fig.5). Quantification of the signal intensity in FIJI (Schindelin et al., 2012) showed that, compared to the control, *αGFP-SPOP* injection reduced the sfGFP-β-catenin protein concentration by 70 %, proving that the Nb-SPOP degradation tool is functional and specific.

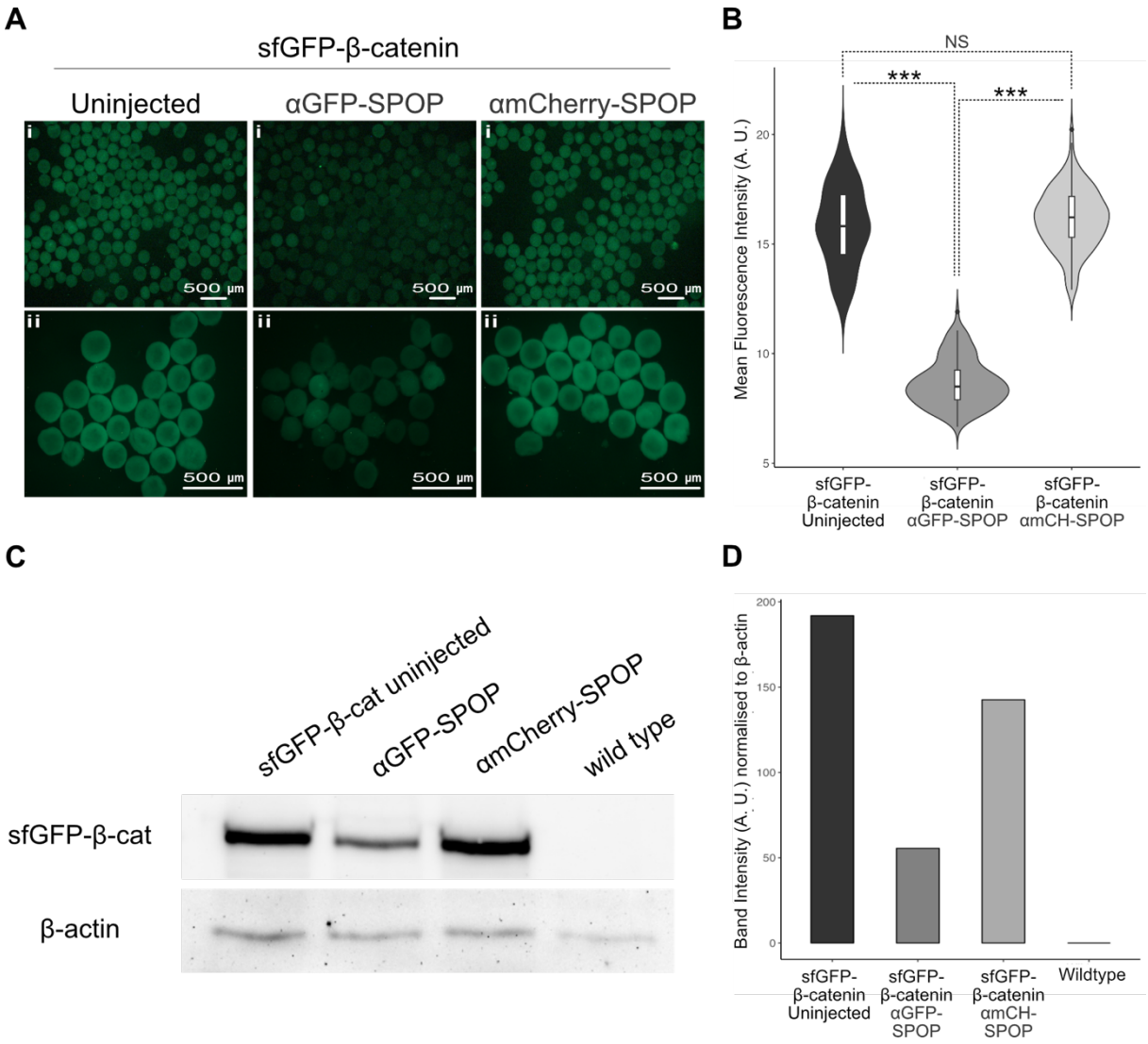

Fig. 5. αGFP-SPOP mediated degradation of sfGFP-β-catenin demonstrated by the reduction of fluorescence intensity and sfGFP-β-catenin concentration upon injection of *αGFP-SPOP* mRNA. **(A)** Images of *sfGFP-β-catenin* transgenic embryos 24hpf. These were used for measuring the change of fluorescence intensity (i) or western blotting (ii). Embryos were either uninjected or injected with *αGFP-SPOP* or *αmCherry-SPOP* mRNA. **(B)** Mean fluorescence intensity of the different samples depicted in (A, i) (n = 130-160). The fluorescence intensity of αGFP-SPOP injected embryos is significantly reduced compared to both control groups (p-value < 0.001). The difference between the control groups is non-significant (p-value > 0.05) **(C)** Western blot analysis of sfGFP-β-catenin in the three samples depicted in (A, ii) and in untreated wildtype. sfGFP-β-catenin was detected using rabbit polyclonal αGFP (abcam290) antibody. Anti-β-actin antibody was used for loading control. **(D)** Band intensity (normalised to β-actin). Assuming a linear relationship between sample concentration and band intensity, sfGFP-β-catenin concentration is reduced by 70 % upon injection of *αGFP-SPOP* mRNA, compared to the uninjected control. In the negative control sample (αmCH-SPOP), sfGFP-β-catenin concentration is reduced by approx. 25% compared to the uninjected control. However, this is likely due to the small number of embryos used per sample (27 embryos) since no difference between control and negative control was detected in the direct fluorescence measurement (B).

2.1.5 αGFP-SPOP mediates the degradation of maternal sfGFP-β-catenin signal

B-catenin is deposited in the egg as protein and mRNA. Hence, I am not able to distinguish between the degradation of maternal sfGFP-β-catenin protein or sfGFP-β-catenin protein translated from maternal mRNA. However, if the αGFP-SPOP tool is functional in the first hours after fertilisation, it seems likely that it is also tagging maternally deposited fusion proteins for degradation. To assess how soon after injection αGFP-SPOP is active, I examined its effect on the expression of germ-layer-specific marker genes. In *Nematostella*, the endoderm is specified at or prior to 6 hpf (Lebedeva et al., 2021). At this time, a maternal β-catenin signal suppresses endoderm specification at the vegetal pole blastomeres, which correspond to the future ectodermal cells (Lebedeva et al., 2022). As a result, the knockdown of maternal β-catenin leads to the ubiquitous expression of endodermal markers, while oral ectodermal markers are completely abolished (Leclère et al., 2016). This differs from the effect of the suppression of the zygotic Wnt/β-catenin signalling, upon which endoderm specification and gastrulation are normal, and only the ectoderm is severely aboralised (Niedermoser et al., 2022). Therefore, I hypothesised that the degradation of maternal sfGFP-β-catenin mediated by αGFP-SPOP would cause a similar change in gene expression as has been achieved by injecting the translation-blocking morpholino against maternal β-catenin *(*Fig.6) (Leclère et al., 2016). To test this, I performed in situ hybridisation with probes against the endodermal marker *SnailA* and the oral ectoderm marker *FoxA* on *αGFP-SPOP* mRNA injected sfGFP-β-catenin embryos. At the morphological as well as the molecular level, *αGFP-SPOP* mRNA injected embryos phenocopy β-catenin morphants. They developed into blastula-like spheres that ubiquitously expressed *SnailA* and completely downregulated *FoxA* (Fig.6). Thus, the molecular identity of all cells in the embryo was converted to endoderm, as expected upon inhibition of the maternal β-catenin signal. Curiously, in a few embryos, *SnailA* expression was confined to approximately two-thirds of the animal. I suspect that these animals were unintentionally injected with a lower dose of *αGFP-SPOP* mRNA since the injection of a low dose of β-catenin morpholino results in a similar phenotype (Leclère et al., 2016). A low amount of residual β-catenin is necessary and sufficient to activate aboral ectoderm pattering transcription factors such as *Six3/6* (Lebedeva et al., 2021; Leclère et al., 2016), suggesting that the *SnailA*-negative region of the low-dose *αGFP-SPOP* injected embryos may correspond to the aboral ectoderm. This, however, will need to be specifically tested in the future. Together, these results confirm that the synthetic BTB protein αGFP-SPOP effectively targets maternally deposited sfGFP-β-catenin, causing a typical β-catenin loss-of-function phenotype.

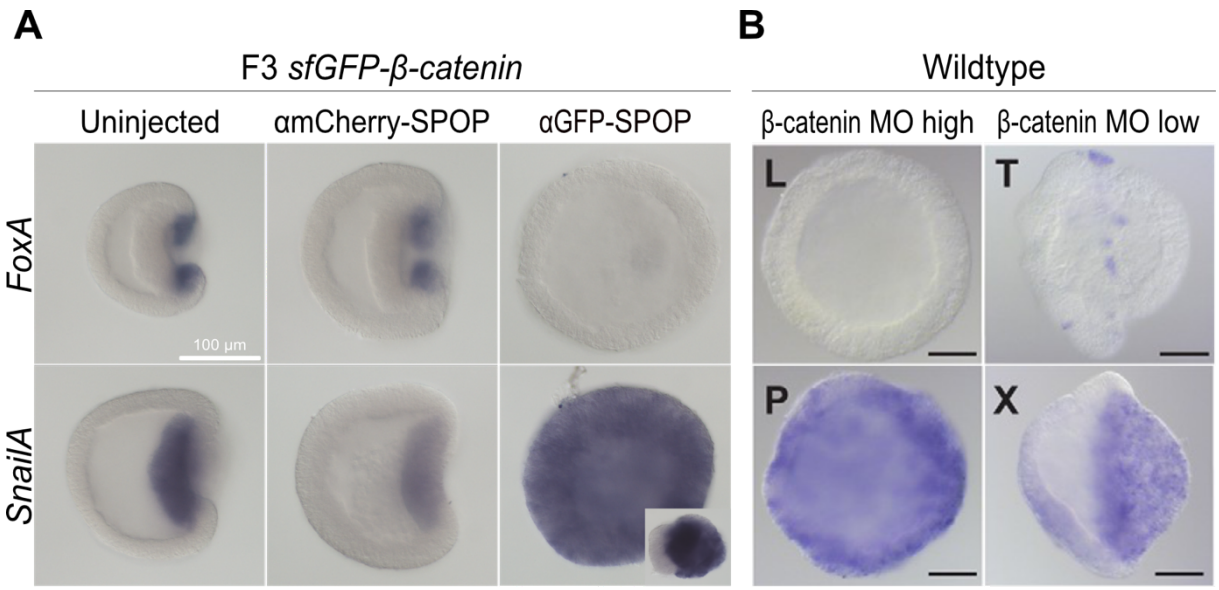

Fig. 6. *αGFP-SPOP injected sfGFP-β-catenin* embryos phenocopy β-catenin morphants. ***(A)*** *αGFP-SPOP* mRNA injected *sfGFP-β-catenin* F3 embryos ubiquitously express the endodermal marker *SnailA* and completely downregulate the oral ectodermal marker *FoxA.* In both control groups - uninjected or injected with *αmCherry-SPOP* mRNA - *SnailA* and *FoxA* are exclusively expressed in the endoderm or oral ectoderm, respectively. The inset image shows a phenotype that is most likely the result of a lower injection dose of *αGFP-SPOP*, i.e., *SnailA* expression everywhere except in the putative aboral ectoderm. **(B)** *SnailA* and *FoxA* expression of embryos injected with a high dose (500 µM) and low dose (100 µM) of *β-catenin* morpholino. All images in B are from Leclère et al. (2016). Lateral views, oral to the right. Embryos are gastrulae at 24hpf.

2.1.6 αmCherry-SPOP injection decreases mCherry signal at 48hpf

To test the αmCherry-SPOP tool, I first used a transgenic line containing a TATA-binding protein (TBP) promoter upstream of the *mCherry* gene (TBP::mCherry) (provided by Yehu Moran). I injected F2 *TBP::mCherry* zygotes with *αmCherry-SPOP* mRNA and compared their fluorescence intensity to a control group injected with *αGFP-SPOP* mRNA. No significant difference between the fluorescence intensity of both groups was detected (Fig.7). Suspecting that this might be due to the αmCherry-SPOP-mediated mCherry degradation being masked by a high amount of mCherry protein, I injected wild-type zygotes with a minimal amount of *mCherry* mRNA together with either *αmCherry-SPOP* or *αGFP-SPOP* mRNA. At 24 hpf, the fluorescence intensity was the same between both groups. However, at 48 hpf, a small but statistically significant decrease in fluorescence intensity was measured in the *αmCherry- SPOP* injected animals (Fig. 6). This shows that the αmCherry-SPOP tool is functional in principle. However, further tests are necessary to fully determine the extent to which mCherry protein or a fusion protein tagged with mCherry can be degraded.

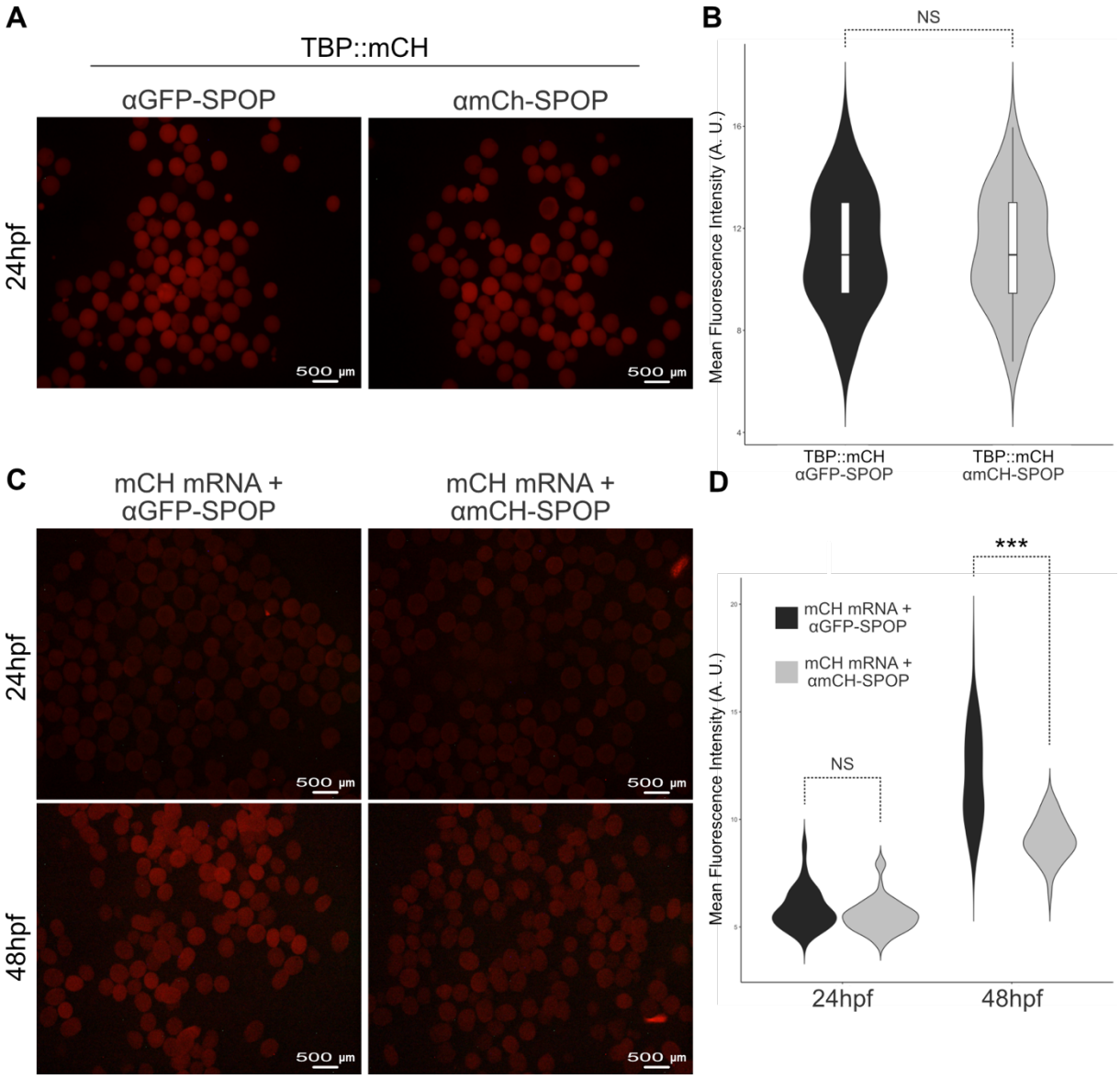

Fig.7. Wildtype zygotes co-injected with *αmCherry-SPOP* and *mCherry* mRNA show a minimal but statistically significant decrease of fluorescence intensity at 48 hpf compared to the control. The fluorescence intensity of *TBP::mCherry* F2s seems not to be affected by *αmCherry-SPOP* mRNA injection. (A) Images of *TBP::mCherry* F2 embryos at 24hpf. Embryos were either injected with *αmCherry-SPOP* mRNA or *αGFP-SPOP* mRNA. **(B)** Mean fluorescence intensity of the samples depicted in (A) (approx. 100 embryos per image). The fluorescence intensity is not significantly different between the two groups (p-value > 0.5) **(C)** Images of wild-type zygotes at 24 hpf and 48 hpf, injected either with *αmCherry-SPOP* mRNA + *mCherry* mRNA or *αGFP-SPOP* mRNA + *mCherry* mRNA. **(D)** Mean fluorescence intensity of the different samples depicted in (C) (approx. 100-150 embryos per image). The fluorescence intensity is not significantly different between the 24hpf groups (p-value > 0.5) and significantly different between the 48 hpf groups (p-value < 0.001).

2.2 Generating knock-in lines for *Hox* genes and *Gbx*

2.2.1 Guide RNA efficacy is a critical yet uncertain factor

My second objective was to generate knock-in lines using CRISPR/Cas9-mediated genome editing. I intended to N- or C-terminally tag the directive axis patterning genes *HoxDa, HoxB,* and *Gbx* in-frame with either *mCherry, GFP, or mCerulean* (Fig.8). To start with, I used CHOPCHOP to select guide RNAs (gRNA) (Labun et al., 2019) (Table S1). The selection was primarily based on the gRNA having a target site near the start or stop codon of the respective gene. If multiple gRNAs met that criterion, I opted for those with the highest predicted efficacy, i.e., its ability to successfully direct Cas9 to the PAM region adjacent to the targeted site. Several factors, including the specific nucleotide in each of the four positions of the seed region (nt 16-20), the presence of poly-N motifs, or the GC content, have been implicated in influencing the efficacy of a gRNA (Konstantakos et al., 2022). Prediction algorithms are trained to take these and many more factors into account. However, as a gRNA is also heavily influenced by the cellular environment and the experimental conditions, algorithms can facilitate the initial gRNA selection but do not guarantee its ultimate in-vivo effectiveness. Practical assessment with, e.g., qPCR melt curve analysis, is still necessary.

2.2.2 *HoxDa, HoxB and Gbx* C-terminal gRNAs are more effective than N-terminal ones

I used qPCR melt curve analysis to assess gRNA efficacy. First, I tested two N-terminal targeting gRNAs per gene. For each gRNA, I assessed genomic DNA extracted from eight individual injected polyps per qPCR run and compared these to the genomic DNA of two control uninjected polyps. All N-terminal gRNAs were functional. However, whereas the Gbx gRNAs proved to be the most effective with an efficacy of 71% and 100%, the HoxDa gRNAs, on the other hand, had an efficacy of only 50%, and the HoxB gRNAs were even less effective with an efficacy below 15% (Fig.8). Subsequent attempts of N-terminal knock-in using these gRNAs remained unsuccessful. Therefore, I assessed another gRNA per gene, this time with a target site close to the C-terminus. Moreover, I increased the sample size to 24 injected polyps per qPCR run to ensure a more robust analysis. These were then compared to eight control uninjected polyps. Both the *HoxDa* and *Gbx* gRNA had an efficacy of over 95 %. The melt curve analysis of *HoxB* gRNA was inconclusive. However, sequencing of ten randomly chosen *HoxB* samples confirmed indels in all but one. These results show that, in the case of *HoxDa*, *HoxB*, and *Gbx*, the tested C-terminal targeting gRNAs are significantly more effective than the N-terminal ones**.**

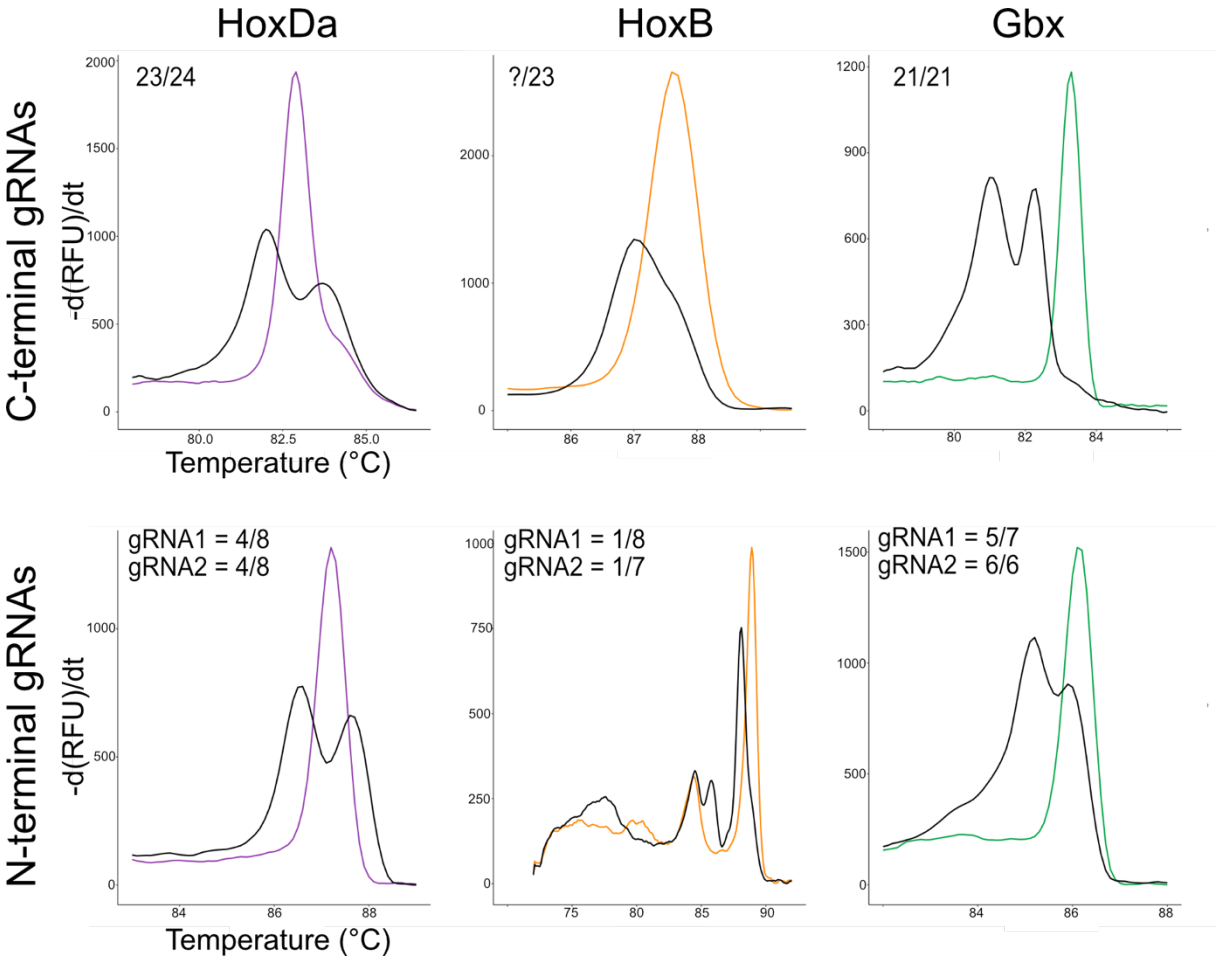

Fig. 8 qPCR melt curves analysis of *HoxDa*, *HoxB*, and *Gbx* gRNAs with N- and C-terminal target sites. Each plot shows the melt curve of one gRNA/Cas9 injected polyp (black curve) plotted together with the melt curve of an uninjected control polyp (coloured curve). The numbers in the top left corner are the ratios between mutant curves and curves identical to the control. The sample size for the N-terminal gRNA assessment was eight injected embryos and two control embryos, and the sample size for the C-terminal gRNA assessment was 24 injected embryos and eight control embryos per qPCR run. Samples in which the PCR amplification failed were not considered. The remaining melt curve plots are shown in Fig. S2-S7. Y-axis = negative first derivative of the change of fluorescent signal over time. X-axis = temperature in Celsius.

2.2.3 HoxDa was successfully tagged in-frame with mCherry

Following the assessment of either N-terminal or C-terminal gRNAs, I assembled the homology-directed repair (HDR) donor templates. The linear HDR donors are comprised of the coding sequence of the reporter, a G4S or G2SG2S flexible linker, and the homology arms (Fig.9). I designed HDR templates bearing long (800-1000bp) homology arms as well as short (20-30 bp) homology arms. To insert the reporters either directly downstream of the start codon or upstream of the stop codon, I injected zygotes with a mix containing the specific HDR template together with the respective gRNA and Cas9 nuclease. Starting at 72hpf, I

screened for fluorescent patches that suggest in-frame HDR donor template knock-in. Ultimately, tagging of HoxB and Gbx was unsuccessful. However, using an HDR template bearing long homology arms, I successfully tagged HoxDa with mCherry at its C-terminus. This was confirmed by Sanger sequencing of three embryos showing clear fluorescent patches in the endoderm, which fits the published *HoxDa* expression pattern (Fig.9, Fig. S8,) (He et al., 2018). The 25 remaining putative transgenic embryos were raised and are currently being crossed with wild-types. The F1s will then be genotyped to select the heterozygous *HoxDa-mCherry* animals.

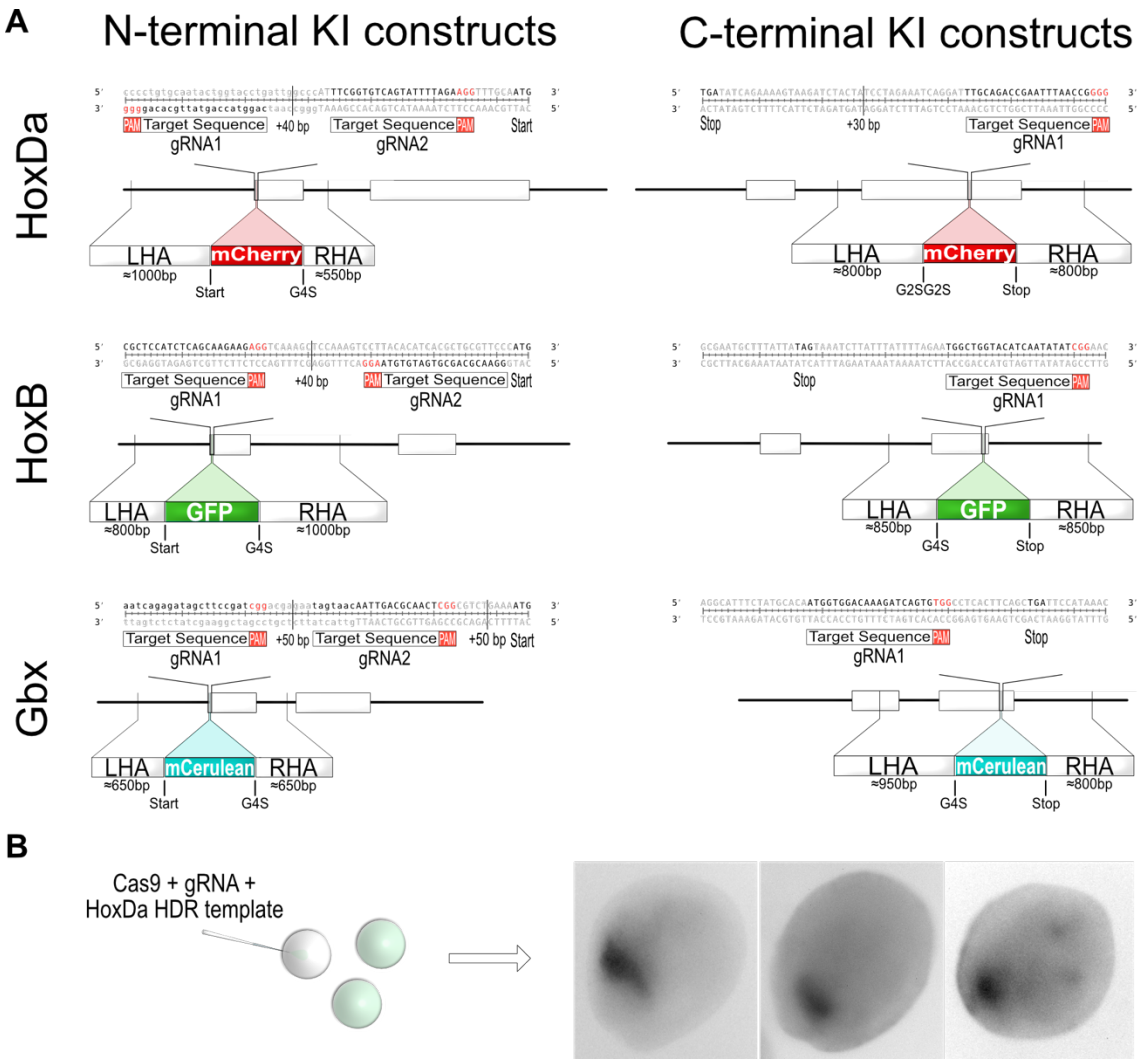

Fig. 9 (A) Schematic representations of the N- and C-terminal knock-in constructs, including *HoxDa*, *HoxB*, and *Gbx* genes, homology-directed repair templates, and gRNA target sites. **(B)** Generation of *HoxDa-mCherry* knock-ins. Embryos were injected with a KI mix containing Cas9, gRNA with a target site near the C-terminus of HoxDa, and the HoxDa homology-directed repair template. Images show planulae with clear mCherry signal (inverted image; fluorescent mCherry appears black).

3. Discussion

3.1 The αmCherry-SPOP tool needs to be tested further

Here, I showed that the Nb-SPOP tool mediates the degradation of fusion proteins in *Nematostella*. As a proof of principle, I injected *sfGFP-β-catenin* F3 zygotes with *αGFP-SPOP* mRNA. αGFP-SPOP significantly reduced the concentration of sfGFP-β-catenin protein, resulting in a typical maternal β-catenin loss-of-function phenotype. In addition, I tested the same degradation tool but with an αmCherry instead of an αGFP nanobody. For that, I injected *TBP::mCherry* F2 zygotes with *αmCherry-SPOP* mRNA and wild-type zygotes with a mix containing *αmCherry-SPOP* mRNA and a low amount (5ng/µl) of *mCherry* mRNA. In the latter, I could detect a small but statistically significant decrease in the fluorescence signal at 48 hpf compared to the control. However, the fluorescence of *TBP::mCherry* transgenics seems not to be affected by αmCherry-SPOP. Since TBP is a ubiquitous and constitutively active promoter, driving *mCherry* expression in 60 % of all cells of a 4-day planula larva and in 90 % of all cells of primary and adult polyps (Admoni et al., 2020), I suspect that mCherry protein is present in significant molar excess, completely masking the αmCherry-SPOP-mediated mCherry degradation. Ultimately, the best system for testing the αmCH-SPOP tool is a knock-in line. It guarantees an endogenous level of the fusion protein and allows further functional analysis upon loss of the specific fusion protein. Recently, our lab obtained transgenic adult *Nematostella* polyps in which endogenous β-catenin is tagged in-frame with mCherry (provided by the Röttinger lab). Once these animals are ready to be induced to spawn, they will be the ideal system for testing the functionality of αmCH-SPOP. If the efficiency of the αmCherry-SPOP construct proves to be insufficient, other αmCherry nanobodies should be tested together with SPOP, which, as I have shown in the case of the αGFP nanobody, works very well.

3.2 Nb-SPOP utility is limited by it requiring a knock-in line

Nb-SPOP-mediated protein degradation can become a valuable tool for studying the function of maternally deposited proteins. However, its use depends on the availability of knock-in lines in which the proteins of interest are tagged in-frame with fluorescent reporters. In *Nematostella,* knock-in was recently done by, e.g., Lebedeva et al. (2022), who, as also described here, generated a *sfGFP-β-catenin* line that finally enabled the precise visualisation of maternal β-catenin protein and the zygotic β-catenin gradient*,* or by Paix et al. (2023) who successfully tagged six different endogenous proteins, achieving knock-in rates of up to 37% and germline transmission for all but one of the targeted loci. Their knock-in protocols differ

mainly in that Paix et al. use a higher concentration of all reagents in the knock-in mix (1.6x gRNA, 4.5x Cas9, 4.2x HDR template) as well as HDR templates bearing short homology arms (15-30 bp) instead of long ones (1000bp). To tag HoxDa, HoxB, and Gbx, I tested both protocols. In my hands, the "high concentrations" knock-in mix significantly increased embryo lethality and did not result in any knock-in. Similarly, increasing the concentration of any single reagent within the knock-in mix and using short homology arm HDR templates together with a "high concentration" or "low concentration" mix had no impact on the knock-in rate. Given that I was able to tag HoxDa with mCherry following the protocol of Lebedeva et al., i.e., HDR templates bearing long homology arms as well as a "low concentration" knock-in mix (as described in Methods 4.7), I consider this to be the more efficient protocol and do not see any benefits in using higher concentrations of the knock-in reagents. However, to fully assess this, it would be necessary to repeat the knock-ins shown by Paix et al. using both protocols. Taken together, while promising progress is being made in using CRISPR/Cas9-mediated gene knock-in*,* it remains a challenging, often futile process that requires further optimisation in *Nematostella.*

3.3 Using Kelch-like 12 to study the function of Dishevelled

According to Lee et al. (2007), maternal Dishevelled is localised at the animal pole. Curiously, this is, as we know now, on the opposite side of the maternal β-catenin signal (Lebedeva et al., 2022). To understand the function of maternal Dishevelled, our lab is currently generating a *Dishevelled-mCherry* knock-in line. Until the line is established and the Nb-SPOP tool can be used to manipulate Dishevelled, another BTP protein – Kelch-like 12 (KLHL12) – might be a viable alternative. KLHL12 is composed of a BTB motif that binds to Cullin3, a linker sequence, and a kelch-domain consisting of multiple kelch repeats (Angers et al., 2006). In in vitro experiments, the KLHL12-Cullin3 complex was shown to mediate Dishevelled ubiquitination (Angers et al., 2006). Moreover, in both *Xenopus* and zebrafish embryos, overexpression of KLHL-12 by mRNA injection phenocopied Dishevelled morphants. Conversely, the injection of KLHL12 morpholino increased their sensitivity to the activation of Wnt/ß-catenin signalling (Angers et al., 2006). These results indicate that in vertebrates, KLHL-12 negatively regulates Dishevelled by linking it to Cullin3, thereby causing its polyubiquitination and subsequent proteasomal degradation. Using maximum likelihood analysis, I identified an orthologous KLHL12 protein in Nematostella (Fig.10), which could be utilised for future experiments.

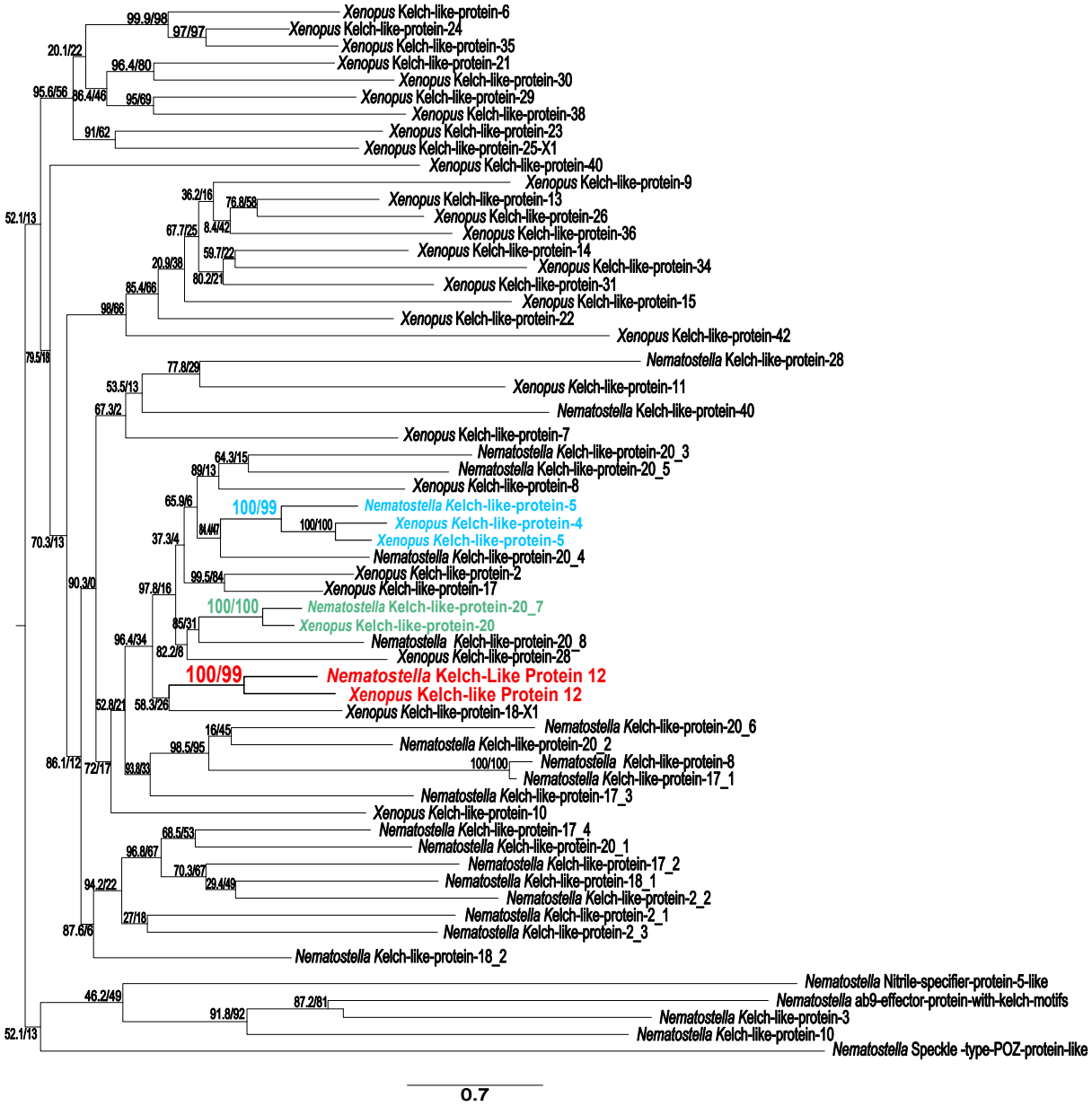

Fig. 10. Maximum likelihood phylogeny of *Nematostella* and *Xenopus* Kelch-like proteins showing robust support for the orthology of *Nematostella* Kelch-like 12 and *Xenopus* Kelch-like 12, Nematostella Kelch-like 20_7 and *Xenopus* Kelch-like 20, and Nematostella Kelch-like 5, Xenopus 5 and Xenopus Kelch-like 4. Numbers indicate the support values for the branches**.** The first number of the node is the result of the SH-aLRT branch test (1000 replicates), and the second number is the bootstrap value (100 replicates). The tree was calculated using IQTREE (substitution model = SQ.pfam + G4 + F). Accession numbers are listed in Table S2

I would use KLHL12 for the following: first, I would overexpress KLHL12 by mRNA injection. To see whether KLHL12 overexpression degrades maternal Dishevelled, I would generate an antibody against *Nematostella* Dishevelled. If maternal Dishevelled is degraded, I would use in-situ hybridisation with probes against the endodermal marker *SnailA* and ectodermal markers *Brachyury* (oral), *Sp6-9* (midbody), and *Six3/6* (aboral) to assess the

phenotype. Examining *SnailA* expression would allow determining whether the loss of maternal Dishevelled affects endoderm specification. In a previous study, Lee et al. (2007) performed a similar experiment to KLHL12 overexpression. They injected a dominant-negative form of Dishevelled (Dishevelled-DIX) and claimed to thereby inhibit endoderm formation and downregulate *SnailA* expression. Their results were in concordance with the then-held belief that β-catenin co-localizes with Dishevelled at the animal pole and activates endoderm specification. This, however, has been refuted by Lebedeva et al. (2022). Moreover, other experiments of the same study could not be replicated in our lab (data not published). Therefore, these experiments need to be repeated. I consider it unlikely that maternal Dishevelled plays a role in endoderm specification for two reasons. First, as described, maternal Dishevelled does not seem to co-localize with maternal nuclear β-catenin. Second, knockdown of *Wnt, Frizzled (Fz),* or *LRP5/6* genes does not affect endoderm specification and gastrulation (Niedermoser et al., 2022). This indicates that Dishevelled may not act as an upstream regulator of maternal β-catenin nuclearisation, as it only inhibits β-catenin degradation upon activation of LRP5/6 and Fz by Wnt. If maternal Dishevelled accumulates at the animal pole, it seems more likely that it acts as a prerequisite for establishing the zygotic β-catenin gradient that patterns the ectoderm along the oral-aboral axis. In this case, the loss of Dishevelled would result in a typical zygotic β-catenin loss-of-function phenotype, i.e., β-catenin-dependent expression of the oral marker *Brachyury* and the midbody marker *Sp6-9* is abolished while the aboral molecular identity marked by *Six3/6* expands throughout the embryo (Lebedeva et al., 2021; Niedermoser et al., 2022). Curiously, the only published loss-of-function experiments on Dishevelled were the ones by Lee et al. (2007), and they did not describe the phenotypes after mid-cleavage. It will be important to fill this knowledge gap and analyse the effect of Dishevelled knockdown on endoderm specification and axial patterning. KLHL12 may also be used, complementary with a Dishevelled antibody (which still needs to be raised), to determine at which pole maternal Dishevelled accumulates. To do so, I would generate a fusion mRNA consisting of *KLHL12* without the BTB motif linked in-frame to *mCherry*. Due to the lack of the BTB motif, KLHL12ΔBTB-mCH should bind to Dishevelled but not tag it for degradation. If this mRNA is injected into *sfGFP-β-catenin* transgenic embryos, and these are then stained with αGFP and αmCherry antibodies, we might be able to determine whether the mCherry and sfGFP-β-catenin signals overlay or, as suggested, are on opposing sides. While these experiments lack the precision of the Dishevelled knock-in line used in combination with the Nb-SPOP tool,

they might still provide a first insight into the function of maternal Dishevelled during the early embryogenesis of *Nematostella.*

3.5 Conclusion

In summary, this work demonstrates a novel tool for studying protein function in *Nematostella*: a modified E3 ubiquitin ligase adapter protein SPOP fused to an αGFP or αmCherry nanobody. By testing the degradation tool on a transgenic knock-in line in which the endogenous β-catenin is tagged in-frame with sfGFP, I showed that *αGFP-SPOP* mRNA injection leads to the targeted degradation of a sfGFP-β-catenin fusion protein. Furthermore, I demonstrated that upon injection of *mCherry* mRNA together with *αmCherry-SPOP*, the mCherry signal is decreased compared to the control. With that, I confirmed the functionality of both Nb-SPOP tools. Compared to the commonly used indirect methods of disrupting protein function, Nb-SPOP provides the advantage of directly targeting the protein, offering an exciting opportunity to analyse the function of previously inaccessible maternally deposited proteins. Additionally, I used CRISPR/Cas9-mediated gene knock-in to successfully tag HoxDa in-frame with mCherry and identified effective gRNAs targeting the C-terminus of HoxB and Gbx, which might enable the generation of further knock-in lines. With this work, I lay the foundation for future research investigating the functional interplay between the directive axis patterning *Hox/Gbx* genes, as well as the function of maternally deposited proteins like Dishevelled in *Nematostella.*

4. Materials and Methods

4.1 Animal culture and microinjection

Adult *Nematostella vectensis* polyps were kept, separated by sex, in the dark at 18°C in 16‰ artificial seawater (Nematostella medium (NM)) and fed five times a week with *Artemia* nauplii. Spawning of individual polyps was induced approximately every three weeks. To do so, they were first thoroughly rinsed with NM and then placed in transparent containers within an illuminated incubator for 9 hours at 25°C. For injection, egg packages were fertilised for 30 minutes and then de-jellied in 3% L-cysteine/NM adjusted to pH 7.4 using sodium hydroxide (NaOH) on a rotary shaker at room temperature (RT) for 15-30 minutes, followed by six washes in NM (for a detailed protocol see Genikhovich and Technau 2009). Microinjection was performed under an inverted fluorescence microscope (Nikon TS100F) using Narishige micromanipulators and an Eppendorf FemtoJet air injection pump as described in (Renfer and Technau, 2017).

4.2 Nanobody-SPOP fusion mRNA

The nanobody-SPOP constructs consist of either an αmCherry or αGFP nanobody fused to a flexible linker and a truncated *Nematostella* Cullin3-RING ubiquitin ligases adaptor protein (Speckle Type BTB/POZ Protein (SPOP) (*Nematostella* gene model NVE12957)) lacking the N-terminal substrate binding domain. The plasmids containing the nanobodies (*pGEX6P1-mCherry-Nanobody*, Addgene plasmid # 70696 ; http://n2t.net/addgene:70696 ; RRID:Addgene_70696) (Katoh et al., 2016), (*pGEX6P1-GFP-Nanobody*, Addgene plasmid # 61838 ; http://n2t.net/addgene:61838 ; RRID:Addgene_61838) (Katoh et al., 2015) were designed by Kazuhisa Nakayama and obtained from Addgene (Watertown, MA, USA). The coding sequences of the nanobodies and SPOP were amplified with primers listed in Table S3. To amplify SPOP, two reverse primers were used to retain or delete the C-terminal nuclear localisation sequence (NLS). The constructs were assembled using overlap extension PCR with the primers containing PacI and SbfI sites and ligated into pJET.1.2 vector (Thermo Fisher Scientific, Waltham, MA). Ligation was performed by mixing 2,5 µl 2x reaction buffer, 0,5 µl pJET vector (50 ng/µl), 1,5 µl DNA and 0,5 µl T4 Ligase (400000 U/ml), and incubating it for 15-30 minutes at RT. The plasmids were then introduced into competent E. coli cells and grown on agar plates containing 0.15 g/ml Ampicillin at 37°C overnight. Plasmid extraction was done using the innuPREP Plasmid Mini Kit 2.0 (Analytik Jena AG) following the manufacturer's instructions. Next, these Nb-SPOP-containing pJet1.2 plasmids, together with a pCRII-TOPO vector containing PacI and SbfI restriction sites, were digested with 0,5 U/µl PacI and 0,5 U/µl SbfI-HF (New England BioLabs) restriction enzymes for 2 hours at 37°C. The excised inserts from the pJet1.2 plasmids and the digested backbone of the pCRII-TOPO were separated by agarose gel electrophoresis at 100 V for 30 minutes in a 1% (w/v) agarose gel in 1 x TAE buffer, purified using the Monarch PCR & DNA Cleanup Kit (NEB, cat. # T1030S), ligated (done as mentioned above with a 1:3 vector to insert ratio), cloned and purified (as mentioned above) (for plasmid maps see Fig. S9). Correct assembly was checked by Sanger sequencing (performed by Microsynth AG) using the primer 5´-ATTTAGGTGACACTATAG-3´ or 5´-TAATACGACTCACTATAGGG-3`. Next, the templates for in vitro transcription were amplified in a 50 µl PCR consisting of 5–15 ng plasmid DNA, 10 µl 5X Q5 Reaction Buffer, 2.5 µl Forward and Reverse Primer (10 µM) each, 1 µl dNTPs (10 mM), 0.25 µl Q5 High-Fidelity DNA Polymerase (2U/µl), and 31.75 µl Milli-Q H2O. Primers used were 5`-TGTAAAACGACGGCCAG-3`and 5`-CAGGAAACAGCTATGAC-3`. The PCR condition was as follows: 95.0° C for 3:00 minutes, 35 cycles of 10 seconds at 95.0° C, 30 seconds at 55.0° C, 50 seconds at 72.0° C,

final extension for 3.00 minutes at 72.0° C and hold at 10°C. The final mRNA was synthesised using the mMESSAGE mMACHINE SP6 Transcription Kit (Invitrogen, Thermo Fisher Scientific, Waltham, MA, cat. # AM1340) and purified with the MEGAclear Transcription Clean-Up Kit (Invitrogen, Thermo Fisher Scientific, Waltham, MA, cat. # AM1908). The mRNA concentration was measured with a NanoDrop 2000 Spectrophotometer.

4.3 Nb-SPOP mRNA injection and quantification of fluorescent intensity

The optimal *Nb-SPOP* mRNA concentration of 150 ng/µl was determined by injecting *Nb-SPOP* mRNA with concentrations ranging from 50 ng/µl to 200 ng/µl and assessing its effectivity (change of fluorescent intensity) and toxicity (survival of the embryos after 48 hours). The final injection mix for all tests on sfGFP-β-catenin embryos and TBP::mCherry embryos consisted of 150 ng/µl *Nb-SPOP* mRNA, 0.5 µl fluorescent dextran (250 ng/µl, AlexaFluor488 or AlexaFluor568), and MiliQ H2O to yield a final volume of 5µl. For co-injection with mCherry mRNA, the mix was the same as above with an additional 5ng/µl mCherry mRNA. Injected embryos and uninjected control embryos were kept at 21°C, washed the following day with NM, and imaged 24 hpf and 48 hpf with a Nikon SMZ18 fluorescent stereomicroscope using a Nikon DS-Fi1 camera and NIS Elements (Nikon) imaging software. Microscope and camera settings were the same between all samples. Quantification of the fluorescent intensity of the embryos was done using FIJI (Schindelin et al., 2012) by encircling each embryo in the images and then measuring the mean brightness within these circles. This was then plotted with R (R Core Team, 2022) using the package ggplot2 (Wickham, 2016).

4.4 Statistical analysis

Statistical tests were performed with R. The normality of the mean fluorescence intensity distributions within each group was evaluated using the Shapiro-Wilk normality test. Following the normality assessment, either a Welch Two Sample t-test or Mann-Whitney U test was used to assess the statistical significance between the mean fluorescence intensities of the different groups. For detailed results see Table S4.

4.5 Western blotting

For each sample, an equal number of embryos was homogenised in 40 µl lysis buffer (Invitrogen, cat. # FNN0011) containing 1x Roche complete protease inhibitor (Roche, cat. #

04693116001). Next, after centrifuging the samples for 10 minutes at 4°C and 16000 rcf, the supernatants were collected, and 10 µl loading dye was added to each sample. Protein lysates were resolved by SDS/polyacrylamide gel electrophoresis (SDS-PAGE) as described by Simpson (2006) and transferred to a nitrocellulose membrane (Thermo Scientific, cat. # 88018). The membrane was washed with PTw (1x PBS (1.86 mM NaH_2PO_4, 8.41 mM Na_2HPO_4, 0.175 M NaCl, pH 7,4) and 0.1% Tween 20) and then blocked with blocking solution (5 % skimmed milk powder in PTw) for 1 hour at RT. After washing with PTw twice for 5 minutes and then twice for 10 minutes (all subsequent washes were done like this), the membrane was incubated with the rabbit polyclonal anti-GFP (abcam290) primary antibody (all antibodies were diluted 1:10000 in blocking solution) at 4°C overnight. The next day, the membrane was washed with PTw, incubated for 1 hour at RT with anti-rabbit IgG conjugated to horseradish-peroxidase, and again washed with PTw. Detection was performed by first incubating the membrane for 5 minutes in SuperSignal West Femto Maximum Sensitivity Substrate (Thermo Fisher Scientific, Waltham, MA,cat # 34095) and subsequent imaging using an EpiChemi 3 Darkroom (UVP BioImaging system, UVP LLC, Upland, CA) and Vision works LS software (Version 6.5.2). Protein size was determined by simultaneously running the Color Prestained Protein Standard, Broad Range (10-250 kDa) marker (New England Biolabs, Ipswich, MA, USA) and scanning the same blot on the same system. For the β-actin loading control, the membrane was stripped using Restore PLUS Western Blot Stripping Buffer according to the manufacturer's instructions (Thermo Fisher Scientific, cat. # 46430) and incubated for 2 hours at RT with rabbit monoclonal anti-β-actin diluted 1:10000 (Cell Signaling Technology, Danvers, MA). Staining with the anti-rabbit IgG conjugated to horseradish-peroxidase, as well as all the washing steps between and after the antibody stainings, as well as HRP activity detection, were performed as described above. The mean intensity of the bands was measured in FIJI and plotted with R using the package ggplot2.

4.6 In-situ hybridisation

In-situ hybridisation was performed mainly as described by Kraus et al. (2016). Briefly, embryos were fixed at either 24 hpf or 48 hpf in 4 % PFA/PBS for 1 hour at RT, washed 5 times in PTw (1x PBS and 0.1% Tween 20), followed by 5 washes in 100% MeOH. They were then stored in 100% MeOH at -20°C. MeOH was gradually removed by a single wash in 50% MeOH/PTw, followed by 3 PTw washes. Next, the embryos were treated with 10 µg/ml proteinase K for 20 minutes. The digestion was stopped with two 4 mg/ml Glycin/PTw washes. The embryos were washed four times in 1% triethanolamine/PTw, with the last two

washes containing 3 µl/ml and 6 µl/ml acetic anhydride. After two PTw washes, they were refixed in 3.7% formaldehyde/PTw for 1 hour, washed 5 times in PTw, transferred into Hybe buffer by a 10 minutes wash in 50% Hybe buffer in PTw (50% formamide, 1% SDS, 5x SSC pH4.5, 100 µg/ ml heparin, 5 mg/ml Torula yeast RNA, 0.1% Tween 20) and another 10 minutes wash in pure Hybe, and then prehybridized at 60°C for 2 hours in Hybe. The samples were then hybridised overnight at 60 °C in Hybe buffer containing 0.5 ng/ml FITC-labeled antisense RNA probe against SnailA or FoxA. After hybridization, the samples were rinsed in Hybe, and the Hybe buffer was diluted stepwise with 2x SSCT through a 60% Hybe / 40% 2x SSCT wash and a 30% Hybe / 70% 2x SSCT wash, both 30 minutes long. This was followed by a 100% 2x SSCT wash for 30 minutes and three 0.2x SSCT washes for 20 minutes each. Until this point, all posthybridization washes were performed at 60°C. After a 10-minute PTw wash at room temperature, the embryos were blocked in a blocking solution (1% Roche blocking reagent in 1x MAB (100mM maleic acid, 150mM NaCl, pH=7.5) for at least 1 hour at RT and then incubated overnight at 4°C with preabsorbed alkaline phosphatase-conjugated Anti-FITC Fab fragments (Roche) diluted 1:2000 in blocking solution. Next, they were washed 10 times in PTw for 15 minutes each at RT, twice in alkaline phosphatase buffer (100mM NaCl, 50mM MgCl2, 10ml Tris, 0.1% Tween-20) for 5 minutes each, and then stained with NBT/BCIP solution (Roche) (4.5 µl NBT and 3.5 µl BCIP per 1 ml AP buffer) at RT in the dark. Staining was stopped by rinsing the embryos with dH2O and washing them in 100% ethanol for several hours. Finally, after a last wash with PTw for up to one hour, the embryos were embedded in 85-87% glycerol overnight, mounted on glass slides the next day, and imaged with a Nikon 80i compound microscope using a Nikon DS-Fi1 camera, and NIS Elements (Nikon) imaging software.

4.7 Phylogenetic analysis

Amino acid sequences of *Xenopus* and *Nematostella* Kelch-like proteins were retrieved using the NCBI BLAST platform and aligned with MUSCLE using Mega11 (Tamura et al., 2021). The maximum likelihood tree (bootstrap 100, SH-aLRT branch test 1000) was calculated using IQTREE (Trifinopoulos et al., 2016). The best-fit substitution model Q.pfam + G4 + F, was determined using Modelfinder in IQTREE (Kalyaanamoorthy et al., 2017).

4.8 Guide RNA/Cas9 injection mix and knock-in injection mix

To assess guide RNA efficacy, zygotes were injected with a gRNA/Cas9 injection mix lacking the HDR donor template. Before preparing the solution, crRNAs (listed in Table S1)

(Alt-R® CRISPR-Cas9 crRNA, 2 nmol) and tracrRNA (Alt-R® CRISPR-Cas9 tracrRNA, 20 nmol, cat. #1072533) were resuspended in Nuclease-Free IDTE Buffer to a final concentration of 100 µM each and stored at -20°C. Next, a 2-part guide RNA complex (crRNA:tracrRNA) was prepared by combining crRNA and tracrRNA in equal volumes (0.8 µl each), heating the mix for 5 minutes at 95°C, and letting it cool down to RT before use. Cas9 Nuclease (Alt-R™ S.p. Cas9 Nuclease V3, 10 µg/µl, 62 µM, cat. #1081058) was diluted to 3.3 µg/µL in Cas9 working buffer (10 mM HEPES pH 7.5, 150 mM KCl). CrRNAs, tracrRNA, Cas9 Nuclease, and Nuclease-Free IDTE Buffer were purchased from Integrated DNA Technologies (IDT) (Coralville, IA, USA). The gRNA/Cas9 injection mix (total volume 6 µl) was prepared by mixing the following reagents: 0.6 µl 10x injection buffer (1 mM Na phosphate buffer, 50 mM KCl), 0.6 µl fluorescent dextran (250ng/ µl, AlexaFluor488 or AlexaFluor568), 1.5 µl gRNA complex (stock conc. 50 µM, final conc. 12.5 µM), 0.6 µl Cas9 (3.3 µg/µl in Cas9 working buffer, final conc. 0.33 µg/µl, 2,06 µM), and 2.7 µl Nuclease Free Water. The injection solution was mixed by pipetting and incubated at 37°C for 15-30 minutes before loading the injection needle. The knock-in injection mix was prepared exactly as the gRNA/Cas9 mix described above, with the only difference being that either 0.1 – 0.2 pmol/µl long homology arm HDR template or 0.4 – 0.8 pmol/µl short homology arm HDR template were added to the mix instead of the Nuclease Free Water.

4.9 Extraction of genomic DNA

Embryos injected with gRNA/Cas9 injection mix and uninjected control embryos were kept at 21°C, washed with NM once a day, and raised until primary polyp stage (6-7 days). Genomic DNA was extracted by first fixing the primary polyps with 3 washes in 100% Methanol (MeOH). Then, each polyp was transferred into a PCR tube, the excess Methanol was aspirated, and the polyps were dried for 20 minutes at 50° C with open tube lids to evaporate any remaining MeOH. Next, the animals were digested in 30 µl of DNA extraction Buffer (10 mM Tris pH8, 1mM EDTA pH8, 25 mM NaCl, 200 µg/ml proteinase K) for 2 hours at 50°C and proteinase K was inactivated by heating it for 10 minutes at 95°C. The unpurified solution resulting from this digest was directly used for the melt curve analysis PCR.

4.10 Melt Curve Analysis

The efficacy of the gRNAs was assessed by melt curve analysis. Melt curves are generated by amplifying sequences that span approximately 100 bp upstream and downstream of the targeted PAM sites. For that, a PCR mix is used that contains an intercalating dye that binds

to double-stranded DNA (dsDNA), and the genomic DNA of wildtypes or embryos that were injected with gRNA/Cas9. The amplicons are then gradually heated, and after every increment of 0.1 °C, the fluorescent signal emitted by the intercalating dye is measured. When the temperature exceeds a specific threshold, dsDNA denatures, and the fluorescent signal decreases concordantly. The melting temperature of DNA depends on its length and specific nucleotide sequence. Indel mutations resulting from Cas9-induced double-stranded breaks change these parameters, causing the mutant melt curve to differ from the control curve. The ratio between the mutant and wild-type curves gives an estimate of the efficacy of a gRNA. Quantitative real-time PCR (qPCR) was performed using the CFX96 Real-Time System with a C1000 Touch Thermal Cycler (Bio-Rad Laboratories, Hercules, CA, USA). The qPCR mix (total volume 10 µl) was as follows: 2 µl genomic DNA, 2 µl 5X Q5 Reaction Buffer (New England Biolabs, Ipswich, MA, USA), 1 µl forward and reverse Primer (10 µM) each, 0.2 µl dNTPs (10 mM), 0.5 µl EvaGreen Dye (Biotium Inc., 20X in Water), 0.05 µl Q5 High-Fidelity DNA Polymerase (2U/ µl) (New England Biolabs, Ipswich, MA, USA), 3.25 µl Nuclease-Free Water. Primers were designed using Primer3 online software (Untergasser et al., 2012) (Table S5). Regarding gRNAs targeting the N-terminus, eight gRNA/Cas9 injected polyps per gRNA and two uninjected control polyps per gene were tested in one qPCR run. For gRNAs targeting the C-terminus, 23 gRNA/Cas9 injected polyps per gRNA and eight uninjected control polyps per gene were tested. The qPCR protocol was as follows: initial denaturation at 95.0° C for 3:00 minutes, followed by 45 amplification cycles of 10 seconds at 95.0° C, 30 seconds of annealing at 60.0° C, and 15 seconds of extension at 72.0° C. A melt curve was then generated by heating the PCR product from 72.0° C to 93.0 °C with an increment of 0.1° C after every plate read. All qPCR runs were analysed using Bio-Rad CFX Maestro 1.1 and Bio-Rad Precision Melt Analysis 1.3 software (Bio-Rad Laboratories, Hercules, CA, USA). Figures were produced with R (R Core Team, 2022) using the package ggplot2 (Wickham, 2016).

4.11 Assembly of the homology-directed repair templates

The homology-directed repair (HDR) donor templates are comprised of the homology arms, i.e., sequences homologous to the upstream and downstream regions adjacent to the CRISPR/Cas9 induced double-stranded break, a G4S or G2SG2S flexible linker to reduce interference of protein folding, and the coding sequence of either mCherry, mCerulean, or GFP. All donor templates were 5′-Biotinylated to impede the formation of DNA concatemers and facilitate single-copy integration (Gutierrez-Triana et al., 2018). Moreover, to prevent the

CRISPR/Cas9 complex from recognising the donor template, the PAM and gRNA spacer sequence of the donor templates were either modified by introducing silent mutations or deleted altogether when positioned in a non-coding region. Donor templates were designed containing either microhomology arms (30bp) or long homology arms (800-1000bp). The former were produced by a simple cloning-free method based on PCR. For this purpose, primers against the cDNA sequence of the desired fluorescent protein were generated with the *Hox/Gbx* gene-specific microhomology arms incorporated at the 5' (Sigma-Aldrich, HPLC purified, 5'-Biotinylated, first 5 phosphodiester bonds of the primer replaced by the phosphorothioate linkages) (Table S6). Amplification was performed in a 50 µl reaction volume as described in Methods 4.2. The PCR setting was as follows: 95.0° C for 3:00 minutes, 35 amplification cycles of 10 seconds at 95.0° C, 30 seconds at 55.0° C, and 45 seconds at 72.0° C, final extension of 3.00 minutes at 72.0° C and hold at 10°C. 3 µl of each of the PCR products were examined using gel electrophoresis at 100 V for 30 minutes in a 1% (w/v) agarose gel in 1 x TAE buffer. The remaining product was purified using the Monarch PCR & DNA Cleanup Kit (NEB, cat. # T1030S). The final concentration was measured with a NanoDrop. Donor templates with long homology arms were synthesised by first amplifying three separate fragments: the upstream and downstream homology arms (800-900 bp each) and the specific reporter gene (CB numbers of plasmids are listed in Table S7). These fragments were then assembled by overlap extension PCR. To amplify the homology arms, primary polyp genomic DNA was extracted by digesting homogenised polyps in 500 µl extraction buffer (100mM Tris pH 8, 150 mM EDTA pH8, 0.5% SDS, Proteinase K (200 µg/ml)) for 2 hours at 50°C. Next, 500 µl Phenol pH8 was added, mixed for 30 seconds, and centrifuged for 10 minutes at 12000 rcf. The upper aqueous phase containing the target DNA was transferred into a fresh tube and mixed with 500 µl Phenol:Chloroform:Isoamyl Alcohol (25:24:1) and again centrifuged for 10 minutes at 12000 rcf. This last step was repeated, and the supernatant was transferred into a fresh tube and mixed with 50 µl of 5 M NaCl. Next, 1 ml of 99 % Ethanol (cooled to -20° C) was added. The precipitating DNA threads were transferred to a fresh tube containing 70 % Ethanol and centrifuged at 4° C at 12000 rcf. Finally, after aspirating the ethanol, the air-dried pellets were redissolved in 50-100 µl 10 mM Tris pH8. To amplify the reporter genes, primers were used containing 15 bp long 5' overhangs complementary to the ends of the homology arm fragments. Each fragment was amplified using the same PCR mix (scaled to 20 µl) as described in Methods 4.2. and purified with the Monarch® DNA Gel Extraction Kit (NEB, cat. #T1020). The HDR templates were then assembled by overlap extension PCR using the forward primer of the left homology arm,

the reverse primer of the right homology arm and an equimolar ratio of all fragments. The final products were cloned into pJet1.2 vectors and submitted for Sanger sequencing (sequencing primers are listed in Table S8) before amplifying them in 50 µl reactions using the 5′Biotinylated primers with five first phosphorothioate bonds 5′-CGAGTTTTTCAGCAAGAT-3′ and 5′-TGTAGGAGATCTTCTAGA-3′. The PCR mix, PCR conditions (extension time changed to 90 seconds at 72° C), and subsequent purification were as described above.

4.12 Genotyping

Screening for successful knock-in was done using a Nikon SMZ18 fluorescent stereomicroscope with appropriate filters starting from three days after injection until primary polyp stage. Embryos with clear fluorescent patches were transferred to a separate petri dish containing NM. A subset of these embryos was genotyped by first extracting genomic DNA (as described for qPCR melt curve analysis) and then performing PCR using primers located in the genomic locus upstream and downstream of the homology arms or upstream of the homology arms and within the insert (Table S9). Products of the right size indicating successful insertion were cloned into pJET1.2 vectors and Sanger sequenced.

6. References

Admoni, Y., Kozlovski, I., Lewandowska, M. and Moran, Y. (2020). TATA Binding Protein (TBP) Promoter Drives Ubiquitous Expression of Marker Transgene in the Adult Sea Anemone Nematostella vectensis. *Genes* **11**, 1081.

Akam, M. (1998). Hox genes, homeosis and the evolution of segment identity: no need for hopeless monsters. *The International journal of developmental biology* **42**, 445–451.

Angers, S., Thorpe, C. J., Biechele, T. L., Goldenberg, S. J., Zheng, N., MacCoss, M. J. and Moon, R. T. (2006). The KLHL12–Cullin-3 ubiquitin ligase negatively regulates the Wnt–β-catenin pathway by targeting Dishevelled for degradation. *Nat Cell Biol* **8,** 348–357.

Chondrogianni, N. and Gonos, E. S. (2012). Structure and Function of the Ubiquitin–Proteasome System. In *Progress in Molecular Biology and Translational Science*, pp. 41–74. Elsevier.

Ciechanover, A. (2015). The unravelling of the ubiquitin system. *Nat Rev Mol Cell Biol* **16,** 322–324.

Crocker, J., Abe, N., Rinaldi, L., McGregor, A. P., Frankel, N., Wang, S., Alsawadi, A., Valenti, P., Plaza, S., Payre, F., et al. (2015). Low Affinity Binding Site Clusters Confer Hox Specificity and Regulatory Robustness. *Cell* **160**, 191–203.

Darras, S., Gerhart, J., Terasaki, M., Kirschner, M. and Lowe, C. J. (2011). β-Catenin specifies the endomesoderm and defines the posterior organizer of the hemichordate *Saccoglossus kowalevskii*. *Development* **138**, 959–970.

De Robertis, E. M. (2008). Evo-Devo: Variations on Ancestral Themes. *Cell* **132**, 185–195.

Diaz-de-la-Loza, M.-C., Loker, R., Mann, R. S. and Thompson, B. J. (2020). Control of tissue morphogenesis by the HOX gene *Ultrabithorax*. *Development* **147**, dev184564.

Doudna, J. A. and Charpentier, E. (2014). The new frontier of genome engineering with CRISPR-Cas9. *Science* **346**, 1258096.

Fire, A., Xu, S., Montgomery, M. K., Kostas, S. A., Driver, S. E. and Mello, C. C. (1998). Potent and specific genetic interference by double-stranded RNA in Caenorhabditis elegans. *Nature* **391**, 806–811.

Fritzenwanker, J. H., Genikhovich, G., Kraus, Y. and Technau, U. (2007). Early development and axis specification in the sea anemone Nematostella vectensis. *Developmental Biology* **310**, 264–279.

Genikhovich, G. and Technau, U. (2009). Induction of Spawning in the Starlet Sea Anemone *Nematostella vectensis* , In Vitro Fertilization of Gametes, and Dejellying of Zygotes. *Cold Spring Harb Protoc* **2009**, pdb.prot5281.

Genikhovich, G. and Technau, U. (2017). On the evolution of bilaterality. *Development* **144**, 3392–3404.

Genikhovich, G., Fried, P., Prünster, M. M., Schinko, J. B., Gilles, A. F., Fredman, D., Meier, K., Iber, D. and Technau, U. (2015). Axis Patterning by BMPs: Cnidarian Network Reveals Evolutionary Constraints. *Cell Reports* **10**, 1646–1654.

Genschik, P., Sumara, I. and Lechner, E. (2013). The emerging family of CULLIN3-RING ubiquitin ligases (CRL3s): cellular functions and disease implications. *EMBO J* **32,** 2307–2320.

Glickman, M. H. and Ciechanover, A. (2002). The Ubiquitin-Proteasome Proteolytic Pathway: Destruction for the Sake of Construction. *Physiological Reviews* **82**, 373–428.

Gutierrez-Triana, J. A., Tavhelidse, T., Thumberger, T., Thomas, I., Wittbrodt, B., Kellner, T., Anlas, K., Tsingos, E. and Wittbrodt, J. (2018). Efficient single-copy HDR by 5' modified long dsDNA donors. *eLife* **7**, e39468.

He, S., del Viso, F., Chen, C.-Y., Ikmi, A., Kroesen, A. E. and Gibson, M. C. (2018). An axial Hox code controls tissue segmentation and body patterning in *Nematostella vectensis*. *Science* **361**, 1377–1380.

Heasman, J. (2002). Morpholino Oligos: Making Sense of Antisense? *Developmental Biology* **243**, 209–214.

Henry, J. Q., Perry, K. J., Wever, J., Seaver, E. and Martindale, M. Q. (2008). β-Catenin is required for the establishment of vegetal embryonic fates in the nemertean, Cerebratulus lacteus. *Developmental Biology* **317**, 368–379.

Hunt, P. and Krumlauf, R. (1992). Hox codes and positional specification in vertebrate embryonic axes. *Annual Review of Cell Biology* **8**, 227–256.

Ju Shin, Y., Kyun Park, S., Jung Jung, Y., Na Kim, Y., Sung Kim, K., Kyu Park, O., Kwon, S.-H., Ho Jeon, S., Trinh, L. A., Fraser, S. E., et al. (2015). Nanobody-targeted E3-ubiquitin ligase complex degrades nuclear proteins. *Sci Rep* **5**, 14269.

Kalyaanamoorthy, S., Minh, B. Q., Wong, T. K. F., von Haeseler, A. and Jermiin, L. S. (2017). ModelFinder: fast model selection for accurate phylogenetic estimates. *Nat Methods* **14**, 587–589.

Katoh, Y., Nozaki, S., Hartanto, D., Miyano, R. and Nakayama, K. (2015). Architectures of multisubunit complexes revealed by a visible immunoprecipitation assay using fluorescent fusion proteins. *Journal of Cell Science* **128**, 2351–2362.

Katoh, Y., Terada, M., Nishijima, Y., Takei, R., Nozaki, S., Hamada, H. and Nakayama, K. (2016). Overall Architecture of the Intraflagellar Transport (IFT)-B Complex Containing Cluap1/IFT38 as an Essential Component of the IFT-B Peripheral Subcomplex. *Journal of Biological Chemistry* **291**, 10962–10975.

Knabl, P., Schauer, A., Pomreinke, A. P., Zimmermann, B., Rogers, K. W., Müller, P. and Genikhovich, G. (2022). Analysis of SMAD1/5 target genes in a sea anemone reveals ZSWIM4-6 as a novel BMP signaling modulator. *bioRxiv*.

Konstantakos, V., Nentidis, A., Krithara, A. and Paliouras, G. (2022). CRISPR–Cas9 gRNA efficiency prediction: an overview of predictive tools and the role of deep learning. *Nucleic Acids Research* **50**, 3616–3637.

Kraus, Y., Aman, A., Technau, U. and Genikhovich, G. (2016). Pre-bilaterian origin of the blastoporal axial organizer. *Nat Commun* **7**, 11694.

Kumburegama, S. and Wikramanayake, A. H. (2007). Specification and patterning of the animal-vegetal axis in sea urchins by the canonical Wnt signaling pathway. *Signal Transduction* **7**, 164–173.

Labun, K., Montague, T. G., Krause, M., Torres Cleuren, Y. N., Tjeldnes, H. and Valen, E. (2019). CHOPCHOP v3: expanding the CRISPR web toolbox beyond genome editing. *Nucleic Acids Research* **47**, W171–W174.

Lebedeva, T., Aman, A. J., Graf, T., Niedermoser, I., Zimmermann, B., Kraus, Y., Schatka, M., Demilly, A., Technau, U. and Genikhovich, G. (2021). Cnidarian-bilaterian comparison reveals the ancestral regulatory logic of the β-catenin dependent axial patterning. *Nat Commun* **12**, 4032.

Lebedeva, T., Boström, J., Mörsdorf, D., Niedermoser, I., Genikhovich, E., Adameyko, I. and Genikhovich, G. (2022). β-catenin-dependent endomesoderm specification appears to be a Bilateria-specific co-option. *bioRxiv*.

Leclère, L., Bause, M., Sinigaglia, C., Steger, J. and Rentzsch, F. (2016). Development of the aboral domain in *Nematostella* requires *β-catenin* and the opposing activities of *six3/6* and *frizzled5/8*. *Development* **143**, 1766–1777.

Lee, P. N., Kumburegama, S., Marlow, H. Q., Martindale, M. Q. and Wikramanayake, A. H. (2007). Asymmetric developmental potential along the animal–vegetal axis in the anthozoan cnidarian, Nematostella vectensis, is mediated by Dishevelled. *Developmental Biology* **310**, 169–186.

Lee, M. T., Bonneau, A. R. and Giraldez, A. J. (2014). Zygotic Genome Activation During the Maternal-to-Zygotic Transition. *Annu. Rev. Cell Dev. Biol.* **30**, 581–613.

Li, X.-M., Wu, H.-L., Xia, Q.-D., Zhou, P., Wang, S.-G., Yu, X. and Hu, J. (2022). Novel insights into the SPOP E3 ubiquitin ligase: From the regulation of molecular mechanisms to tumorigenesis. *Biomedicine & Pharmacotherapy* **149**, 112882.

Logan, C. Y., Miller, J. R., Ferkowicz, M. J. and McClay, D. R. (1999). Nuclear β-catenin is required to specify vegetal cell fates in the sea urchin embryo. *Development* **126,** 345–357.

Mallo, M., Wellik, D. M. and Deschamps, J. (2010). Hox genes and regional patterning of the vertebrate body plan. *Developmental Biology* **344**, 7–15.

McClay, D. R., Croce, J. C. and Warner, J. F. (2021). Conditional specification of endomesoderm. *Cells & Development* **167**, 203716.

Niedermoser, I., Lebedeva, T. and Genikhovich, G. (2022). Sea anemone Frizzled receptors play partially redundant roles in oral-aboral axis patterning. *Development* **149**, dev200785.

Niehrs, C. (2010). On growth and form: a Cartesian coordinate system of Wnt and BMP signaling specifies bilaterian body axes. *Development* **137**, 845–857.

Petroski, M. D. and Deshaies, R. J. (2005). Function and regulation of cullin–RING ubiquitin ligases. *Nat Rev Mol Cell Biol* **6**, 9–20.

R Core Team (2022). R: A language and environment for statistical computing.

Renfer, E. and Technau, U. (2017). Meganuclease-assisted generation of stable transgenics in the sea anemone Nematostella vectensis. *Nat Protoc* **12**, 1844–1854.

Schindelin, J., Arganda-Carreras, I., Frise, E., Kaynig, V., Longair, M., Pietzsch, T., Preibisch, S., Rueden, C., Saalfeld, S., Schmid, B., et al. (2012). Fiji: an open-source platform for biological-image analysis. *Nat Methods* **9**, 676–682.

Sharma, M., Castro-Piedras, I., Simmons, G. E. and Pruitt, K. (2018). Dishevelled: A masterful conductor of complex Wnt signals. *Cellular Signalling* **47**, 52–64.

Simpson, R. J. (2006). SDS-PAGE of Proteins. *Cold Spring Harbor Protocols* **1**, pdb.prot4313.

Tamura, K., Stecher, G. and Kumar, S. (2021). MEGA11: Molecular Evolutionary Genetics Analysis Version 11. *Molecular Biology and Evolution* **38**, 3022–3027**.**

Technau, U. and Genikhovich, G. (2018). Evolution: Directives from Sea Anemone Hox Genes. *Current Biology* **28**, R1303–R1305.

Trifinopoulos, J., Nguyen, L.-T., von Haeseler, A. and Minh, B. Q. (2016). W-IQ-TREE: a fast online phylogenetic tool for maximum likelihood analysis. *Nucleic Acids Res* **44,** W232–W235.

Untergasser, A., Cutcutache, I., Koressaar, T., Ye, J., Faircloth, B. C., Remm, M. and Rozen, S. G. (2012). Primer3—new capabilities and interfaces. *Nucleic Acids Research* **40**, e115–e115.

Wang, S., Jiang, S., Zheng, G. and Cho, Y. K. (2022). Targeted degradation of microtubule-associated protein tau using an engineered nanobody-E3 ubiquitin ligase adapter fusion. *bioRxiv*.

Wellik, D. M. and Capecchi, M. R. (2003). *Hox10* and *Hox11* Genes Are Required to Globally Pattern the Mammalian Skeleton. *Science* **301**, 363–367.

Wickham, H. (2016). *ggplot2: Elegant Graphics for Data Analysis*. New York, NY: Springer New York.

Wikramanayake, A. H., Hong, M., Lee, P. N., Pang, K., Byrum, C. A., Bince, J. M., Xu, R. and Martindale, M. Q. (2003). An ancient role for nuclear b-catenin in the evolution of axial polarity and germ layer segregation. *Nature* **426**, 446–450.

7. Supplementary Information

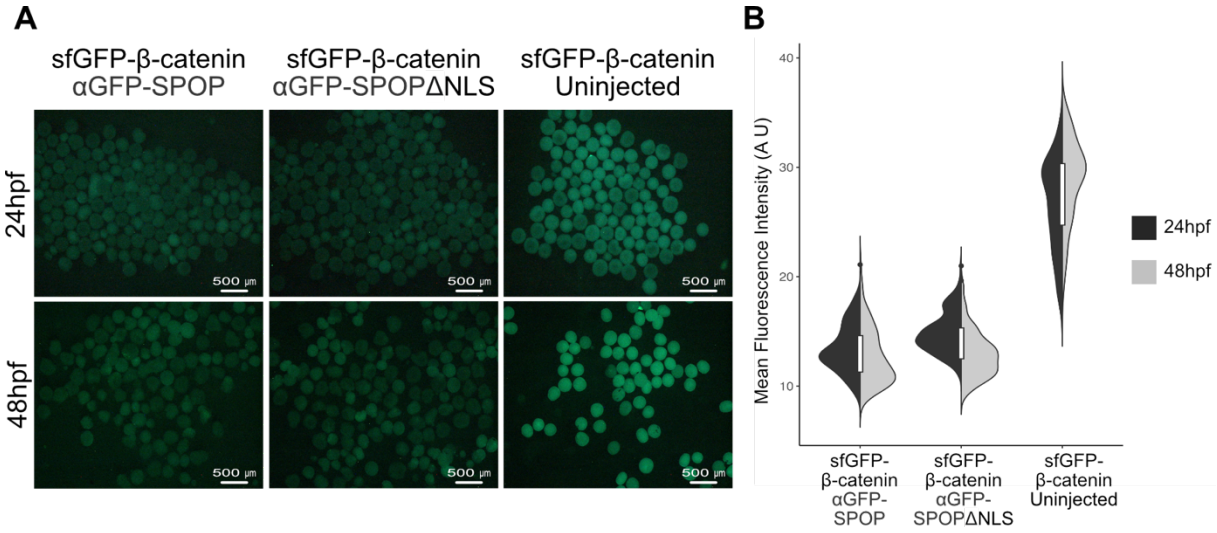

Fig. S1. *αGFP-SPOP* and *αGFP-SPOPΔNLS* mRNA injection reduces the fluorescence intensity of sfGFP-β-catenin embryos. Embryos were either uninjected or injected with *αGFP-SPOP* or *αGFP-SPOPΔNLS* mRNA. **(A)** Images of F3 *sfGFP-β-catenin* transgenic embryos at 24hpf and 48hpf. These were used for measuring the change in fluorescent intensity. **(B)** Mean fluorescent intensity of the different samples depicted in A.

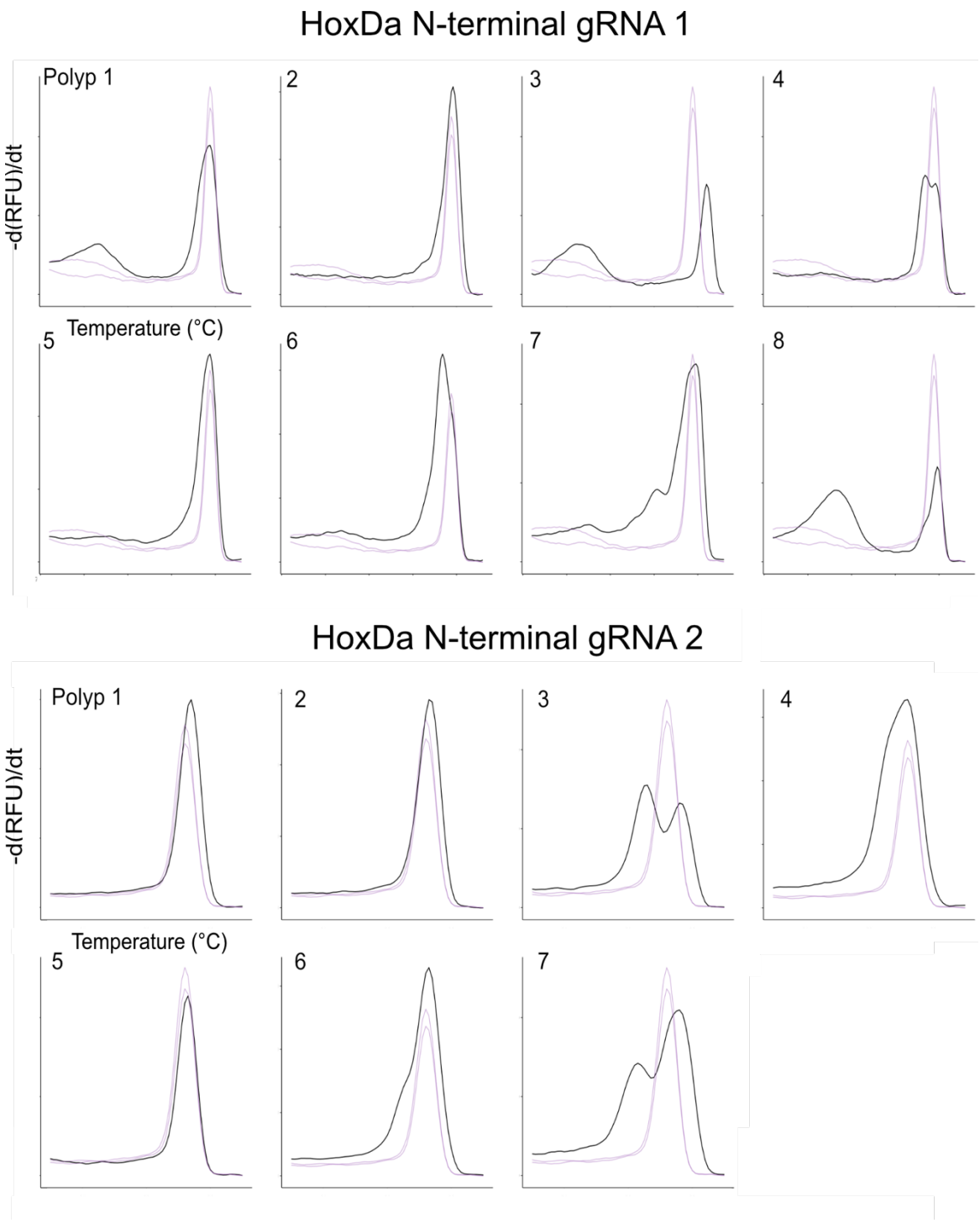

Fig. S2. qPCR melt curves analysis of HoxDa gRNAs with N-terminal target site. Y-axis = negative first derivative of the change of fluorescent signal over time. X-axis = temperature in Celsius. The sample size was eight injected embryos and two control embryos. In each plot, one gRNA/Cas9 injected sample (black curve) is plotted together with both control samples (purple curve). Samples in which the PCR amplification failed are not shown.

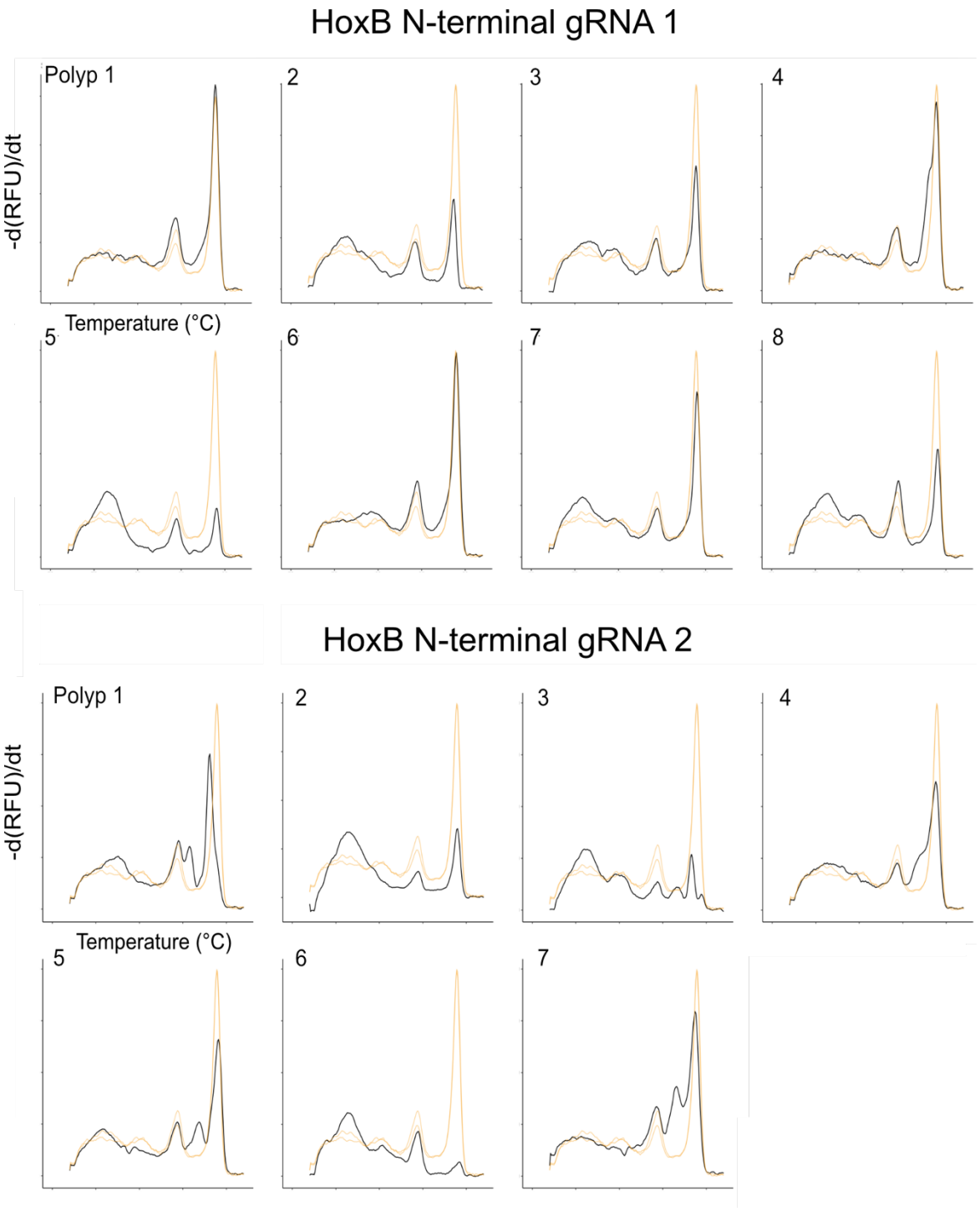

Fig. S3. qPCR melt curves analysis of HoxB gRNAs with N-terminal target site. Y-axis = negative first derivative of the change of fluorescent signal over time. X-axis = temperature in Celsius. The sample size was eight injected embryos and two control embryos. In each plot, one gRNA/Cas9 injected sample (black curve) is plotted together with both control samples (orange curve). Samples in which the PCR amplification failed are not shown.

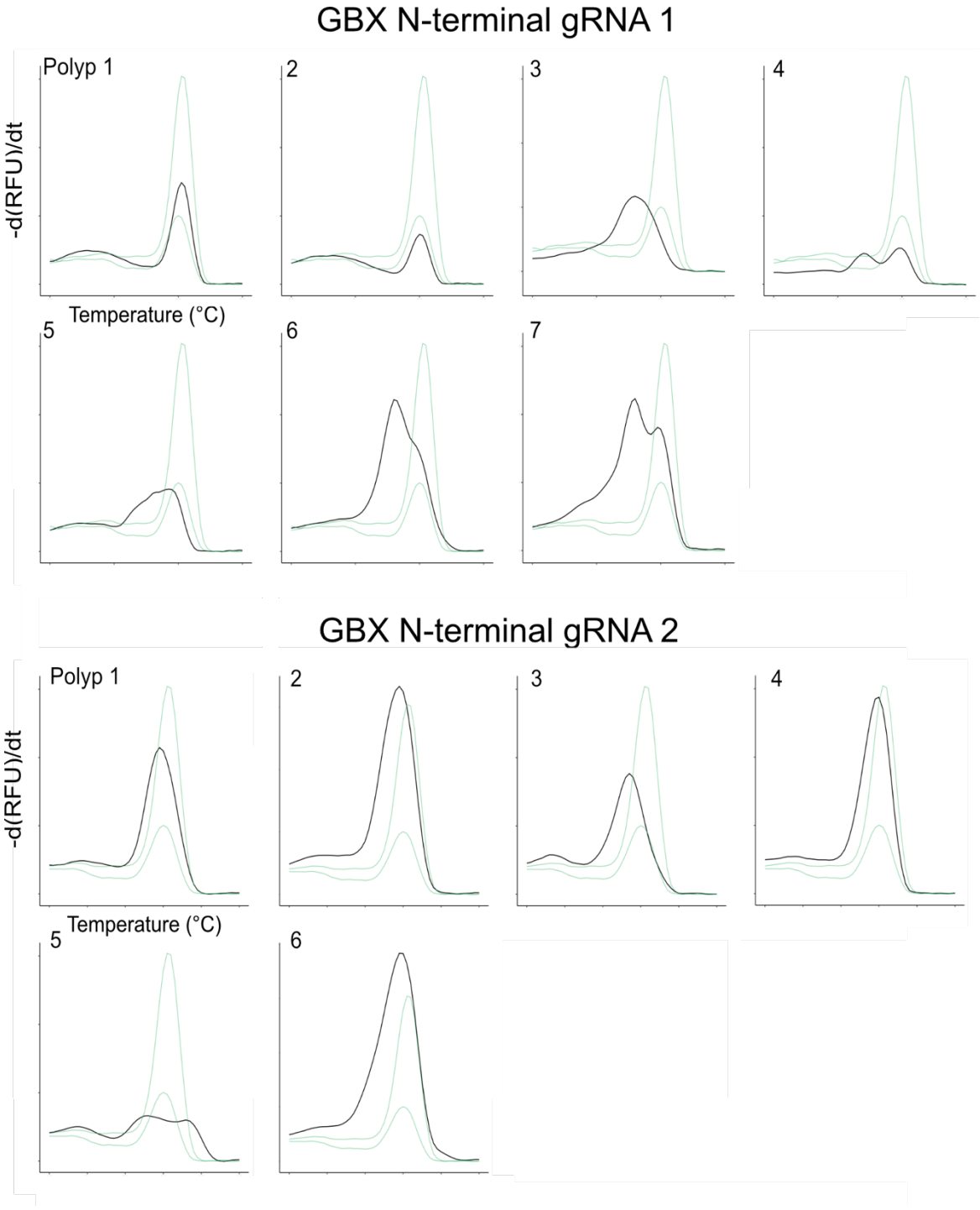

Fig. S4. qPCR melt curves analysis of Gbx gRNAs with N-terminal target site. Y-axis = negative first derivative of the change of fluorescent signal over time. X-axis = temperature in Celsius. The sample size was eight injected embryos and two control embryos. In each plot, one gRNA/Cas9 injected sample (black curve) is plotted together with both control samples (green curve). Samples in which the PCR amplification failed are not shown.

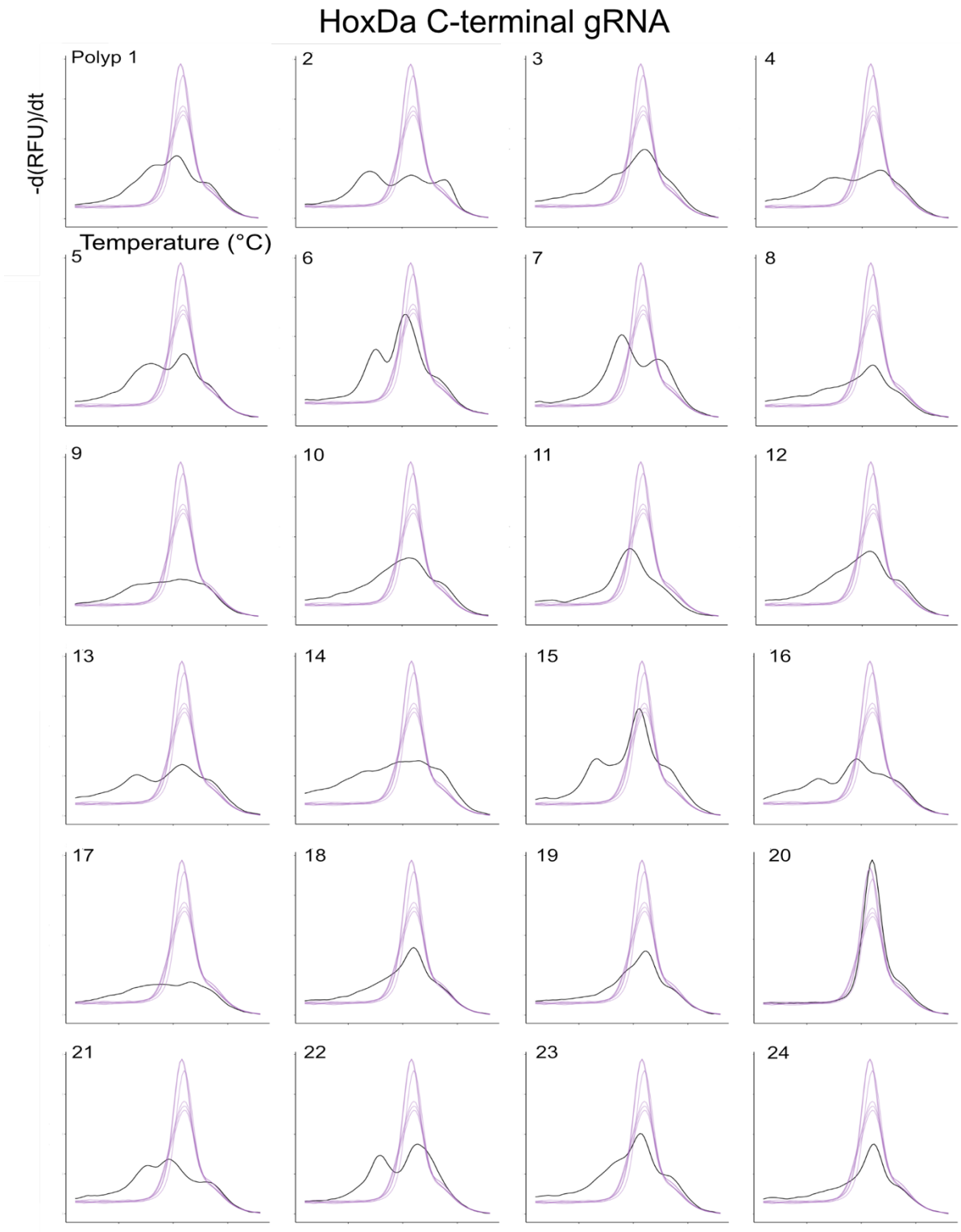

Fig. S5. qPCR melt curves analysis of HoxDa gRNAs with C-terminal target site. Y-axis = negative first derivative of the change of fluorescent signal over time. X-axis = temperature in Celsius. The sample size was 24 injected embryos and eight control embryos. In each plot, one gRNA/Cas9 injected sample (black curve) is plotted together with all control samples (purple curve). Samples in which the PCR amplification failed are not shown.

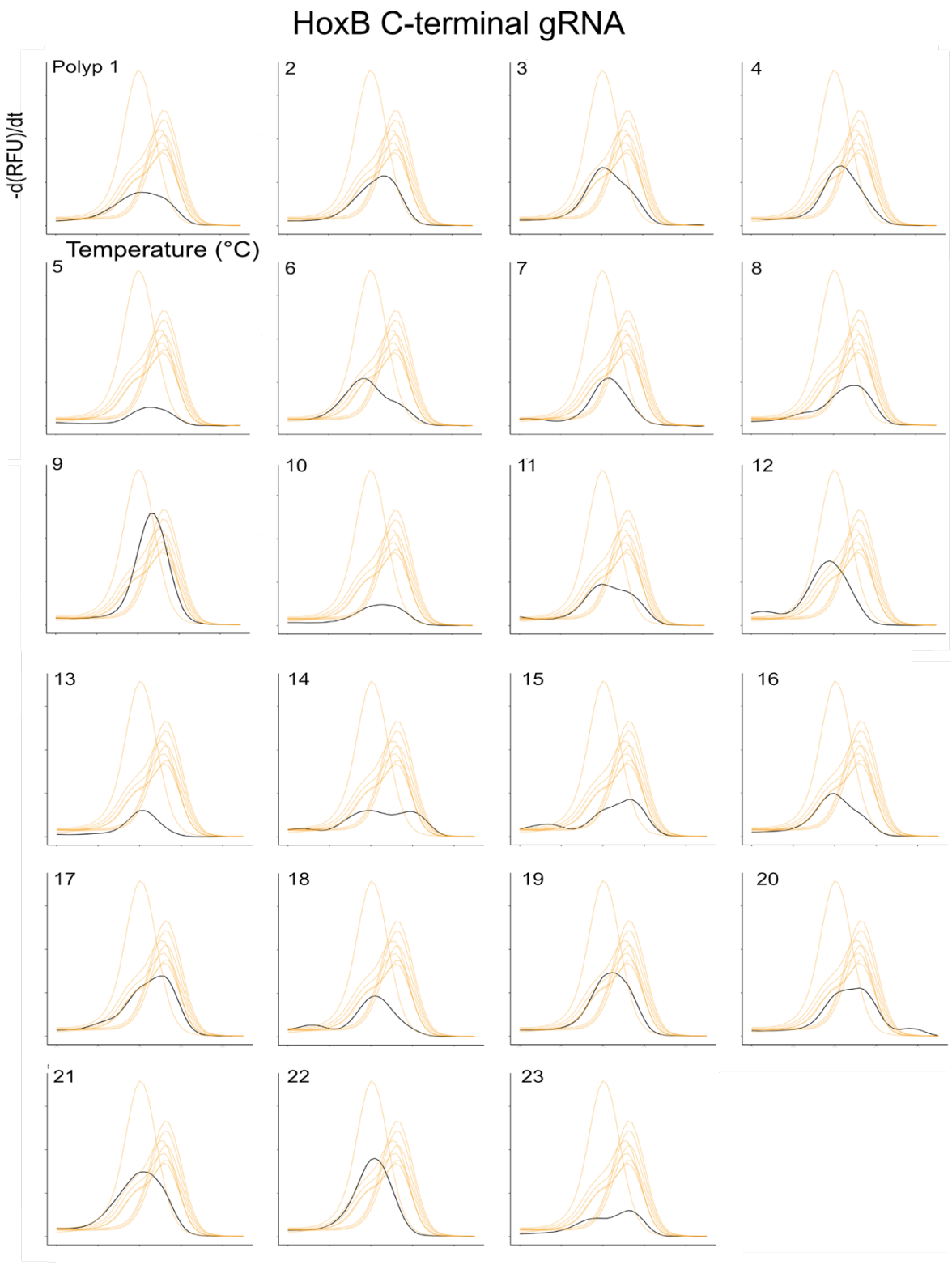

Fig. S6. qPCR melt curves analysis of HoxB gRNAs with C-terminal target site. Y-axis = negative first derivative of the change of fluorescent signal over time. X-axis = temperature in Celsius. The sample size was 24 injected embryos and eight control embryos. In each plot, one gRNA/Cas9 injected sample (black curve) is plotted together with all control samples (orange curve). Samples in which the PCR amplification failed are not shown.

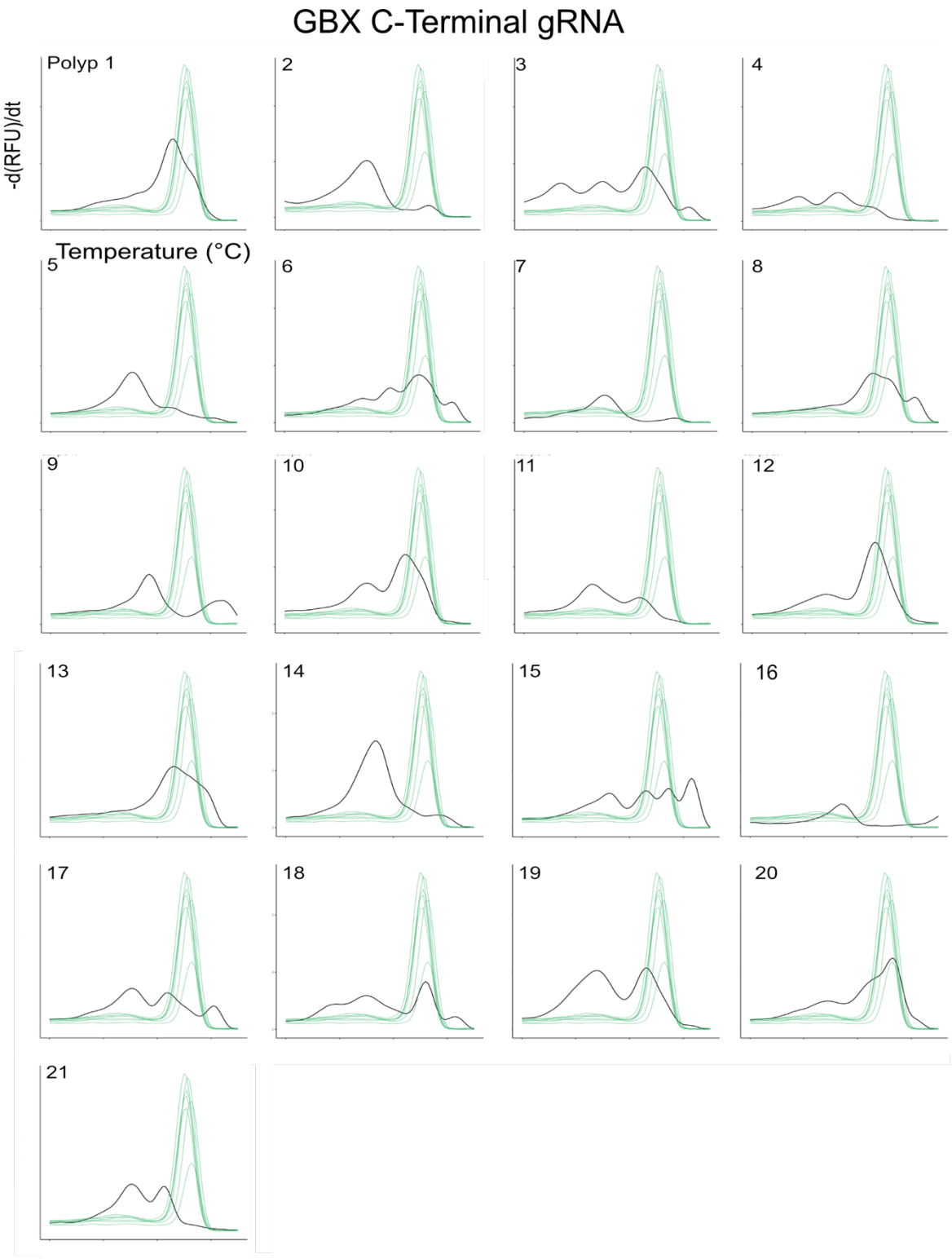

Fig. S7. qPCR melt curves analysis of Gbx gRNAs with C-terminal target site. Y-axis = negative first derivative of the change of fluorescent signal over time. X-axis = temperature in Celsius. The sample size was 24 injected embryos and eight control embryos. In each plot, one gRNA/Cas9 injected sample (black curve) is plotted together with all control samples (green curve). Samples in which the PCR amplification failed are not shown.

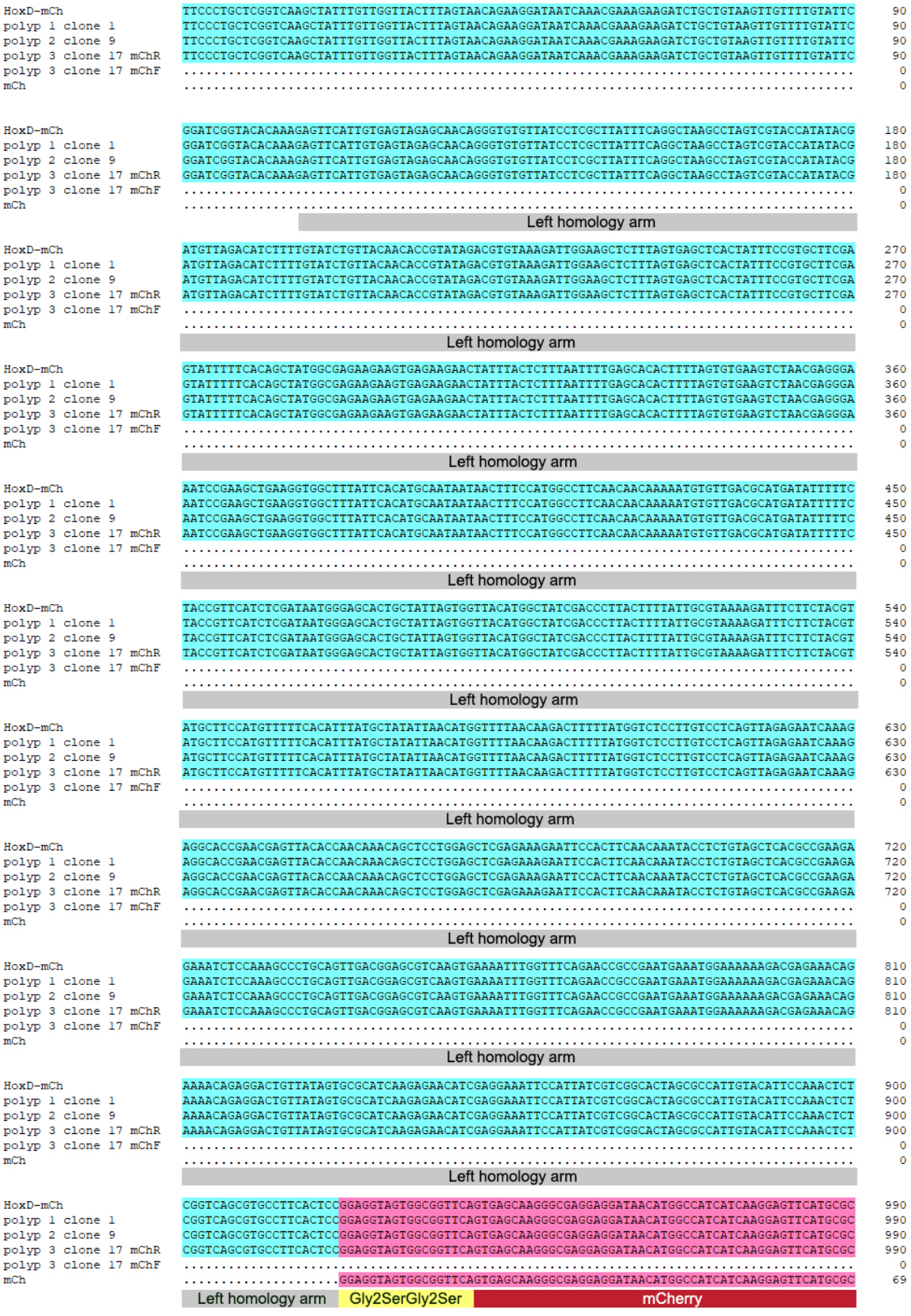
HoxD-mCh
polyp 1 clone 1
polyp 2 clone 9
polyp 3 clone 17 mChR
polyp 3 clone 17 mChF
mCh
Left homology arm
Left homology arm
Left homology arm
Left homology arm
Left homology arm
Left homology arm
Left homology arm
Left homology arm
Left homology arm
Gly2SerGly2Ser
mCherry

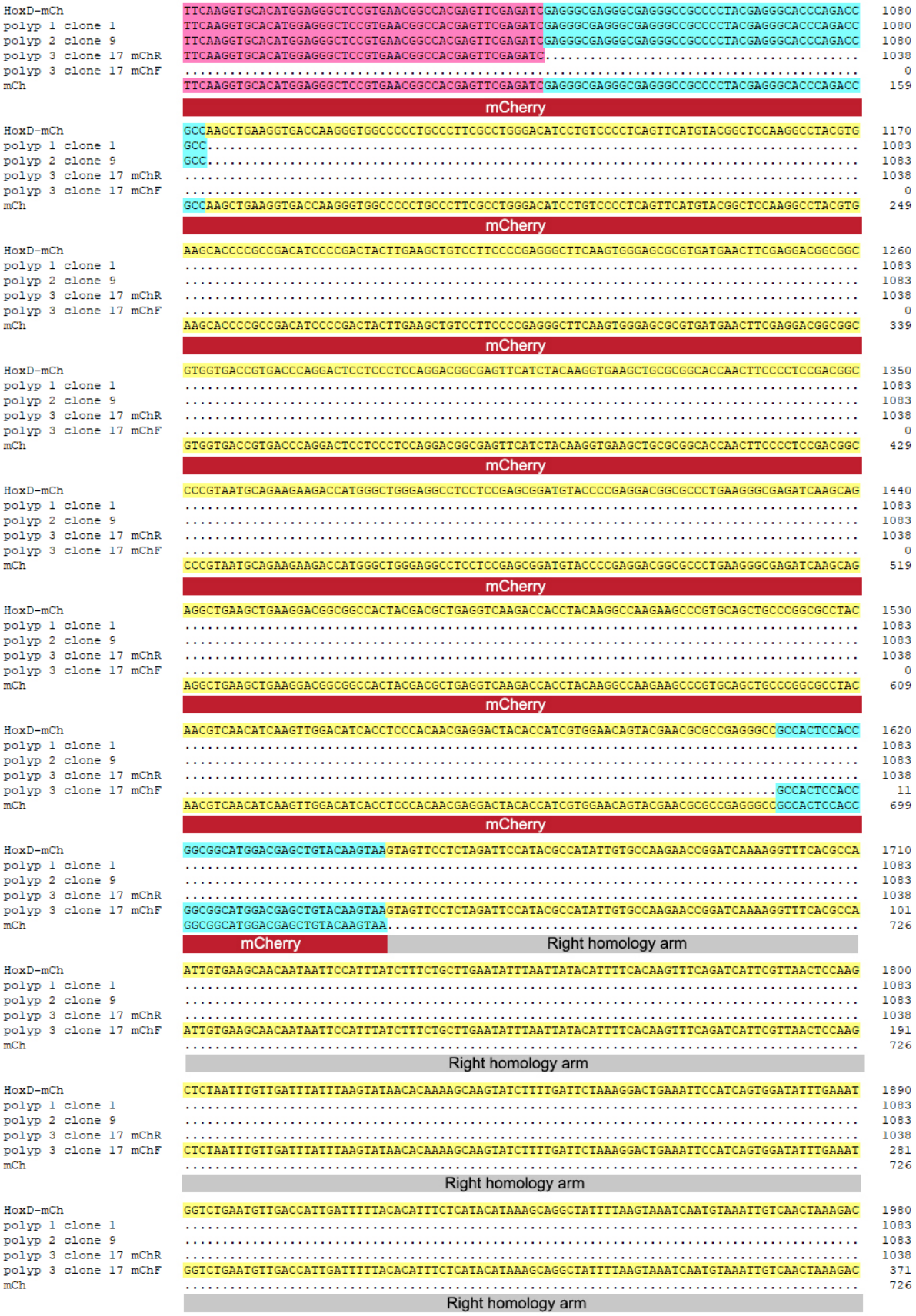
HoxD-mCh TTCAAGGTGCACATGGAGGGCTCCGTGAACGGCCACGAGTTCGAGATCGAGGGCGAGGGCGAGGGCCGCCCCTACGAGGGCACCCAGACC 1080
polyp 1 clone 1 TTCAAGGTGCACATGGAGGGCTCCGTGAACGGCCACGAGTTCGAGATCGAGGGCGAGGGCGAGGGCCGCCCCTACGAGGGCACCCAGACC 1080
polyp 2 clone 9 TTCAAGGTGCACATGGAGGGCTCCGTGAACGGCCACGAGTTCGAGATCGAGGGCGAGGGCGAGGGCCGCCCCTACGAGGGCACCCAGACC 1080
polyp 3 clone 17 mChR TTCAAGGTGCACATGGAGGGCTCCGTGAACGGCCACGAGTTCGAGATC..... 1038
polyp 3 clone 17 mChF 0
mCh TTCAAGGTGCACATGGAGGGCTCCGTGAACGGCCACGAGTTCGAGATCGAGGGCGAGGGCGAGGGCCGCCCCTACGAGGGCACCCAGACC 159
mCherry
HoxD-mCh GCCAAGCTGAAGGTGACCAAGGGTGGCCCCCTGCCCTTCGCCTGGGACATCCTGTCCCCTCAGTTCATGTACGGCTCCAAGGCCTACGTG 1170
polyp 1 clone 1 GCC..... 1083
polyp 2 clone 9 GCC..... 1083
polyp 3 clone 17 mChR 1038
polyp 3 clone 17 mChF 0
mCh GCCAAGCTGAAGGTGACCAAGGGTGGCCCCCTGCCCTTCGCCTGGGACATCCTGTCCCCTCAGTTCATGTACGGCTCCAAGGCCTACGTG 249
mCherry
HoxD-mCh AAGCACCCCGCCGACATCCCCGACTACTTGAAGCTGTCCTTCCCCGAGGGCTTCAAGTGGGAGCGCGTGATGAACTTCGAGGACGGCGGC 1260
polyp 1 clone 1 1083
polyp 2 clone 9 1083
polyp 3 clone 17 mChR 1038
polyp 3 clone 17 mChF 0
mCh AAGCACCCCGCCGACATCCCCGACTACTTGAAGCTGTCCTTCCCCGAGGGCTTCAAGTGGGAGCGCGTGATGAACTTCGAGGACGGCGGC 339
mCherry
HoxD-mCh GTGGTGACCGTGACCCAGGACTCCTCCCTCCAGGACGGCGAGTTCATCTACAAGGTGAAGCTGCGCGGCACCAACTTCCCCTCCGACGGC 1350
polyp 1 clone 1 1083
polyp 2 clone 9 1083
polyp 3 clone 17 mChR 1038
polyp 3 clone 17 mChF 0
mCh GTGGTGACCGTGACCCAGGACTCCTCCCTCCAGGACGGCGAGTTCATCTACAAGGTGAAGCTGCGCGGCACCAACTTCCCCTCCGACGGC 429
mCherry
HoxD-mCh CCCGTAATGCAGAAGAAGACCATGGGCTGGGAGGCCTCCTCCGAGCGGATGTACCCCGAGGACGGCGCCCTGAAGGGCGAGATCAAGCAG 1440
polyp 1 clone 1 1083
polyp 2 clone 9 1083
polyp 3 clone 17 mChR 1038
polyp 3 clone 17 mChF 0
mCh CCCGTAATGCAGAAGAAGACCATGGGCTGGGAGGCCTCCTCCGAGCGGATGTACCCCGAGGACGGCGCCCTGAAGGGCGAGATCAAGCAG 519
mCherry
HoxD-mCh AGGCTGAAGCTGAAGGACGGCGGCCACTACGACGCTGAGGTCAAGACCACCTACAAGGCCAAGAAGCCCGTGCAGCTGCCCGGCGCCTAC 1530
polyp 1 clone 1 1083
polyp 2 clone 9 1083
polyp 3 clone 17 mChR 1038
polyp 3 clone 17 mChF 0
mCh AGGCTGAAGCTGAAGGACGGCGGCCACTACGACGCTGAGGTCAAGACCACCTACAAGGCCAAGAAGCCCGTGCAGCTGCCCGGCGCCTAC 609
mCherry
HoxD-mCh AACGTCAACATCAAGTTGGACATCACCTCCCACAACGAGGACTACACCATCGTGGAACAGTACGAACGCGCCGAGGGCCGCCACTCCACC 1620
polyp 1 clone 1 1083
polyp 2 clone 9 1083
polyp 3 clone 17 mChR 1038
polyp 3 clone 17 mChF .....GCCACTCCACC 11
mCh AACGTCAACATCAAGTTGGACATCACCTCCCACAACGAGGACTACACCATCGTGGAACAGTACGAACGCGCCGAGGGCCGCCACTCCACC 699
mCherry
HoxD-mCh GGCGGCATGGACGAGCTGTACAAGTAAGTAGTTCCTCTAGATTCCATACGCCATATTGTGCCAAGAACCGGATCAAAAGGTTTCACGCCA 1710
polyp 1 clone 1 1083
polyp 2 clone 9 1083
polyp 3 clone 17 mChR 1038
polyp 3 clone 17 mChF GGCGGCATGGACGAGCTGTACAAGTAAGTAGTTCCTCTAGATTCCATACGCCATATTGTGCCAAGAACCGGATCAAAAGGTTTCACGCCA 101
mCh GGCGGCATGGACGAGCTGTACAAGTAA..... 726
mCherry
Right homology arm
HoxD-mCh ATTGTGAAGCAACAATAATTCCATTTATCTTTCTGCTTGAATATTTAATTATACATTTTCACAAGTTTCAGATCATTCGTTAACTCCAAG 1800
polyp 1 clone 1 1083
polyp 2 clone 9 1083
polyp 3 clone 17 mChR 1038
polyp 3 clone 17 mChF ATTGTGAAGCAACAATAATTCCATTTATCTTTCTGCTTGAATATTTAATTATACATTTTCACAAGTTTCAGATCATTCGTTAACTCCAAG 191
mCh 726
Right homology arm
HoxD-mCh CTCTAATTTGTTGATTTATTTAAGTATAACACAAAAGCAAGTATCTTTTGATTCTAAAGGACTGAAATTCCATCAGTGGATATTTGAAAT 1890
polyp 1 clone 1 1083
polyp 2 clone 9 1083
polyp 3 clone 17 mChR 1038
polyp 3 clone 17 mChF CTCTAATTTGTTGATTTATTTAAGTATAACACAAAAGCAAGTATCTTTTGATTCTAAAGGACTGAAATTCCATCAGTGGATATTTGAAAT 281
mCh 726
Right homology arm
HoxD-mCh GGTCTGAATGTTGACCATTGATTTTTACACATTTCTCATACATAAAGCAGGCTATTTTAAGTAAATCAATGTAAATTGTCAACTAAAGAC 1980
polyp 1 clone 1 1083
polyp 2 clone 9 1083
polyp 3 clone 17 mChR 1038
polyp 3 clone 17 mChF GGTCTGAATGTTGACCATTGATTTTTACACATTTCTCATACATAAAGCAGGCTATTTTAAGTAAATCAATGTAAATTGTCAACTAAAGAC 371
mCh 726
Right homology arm

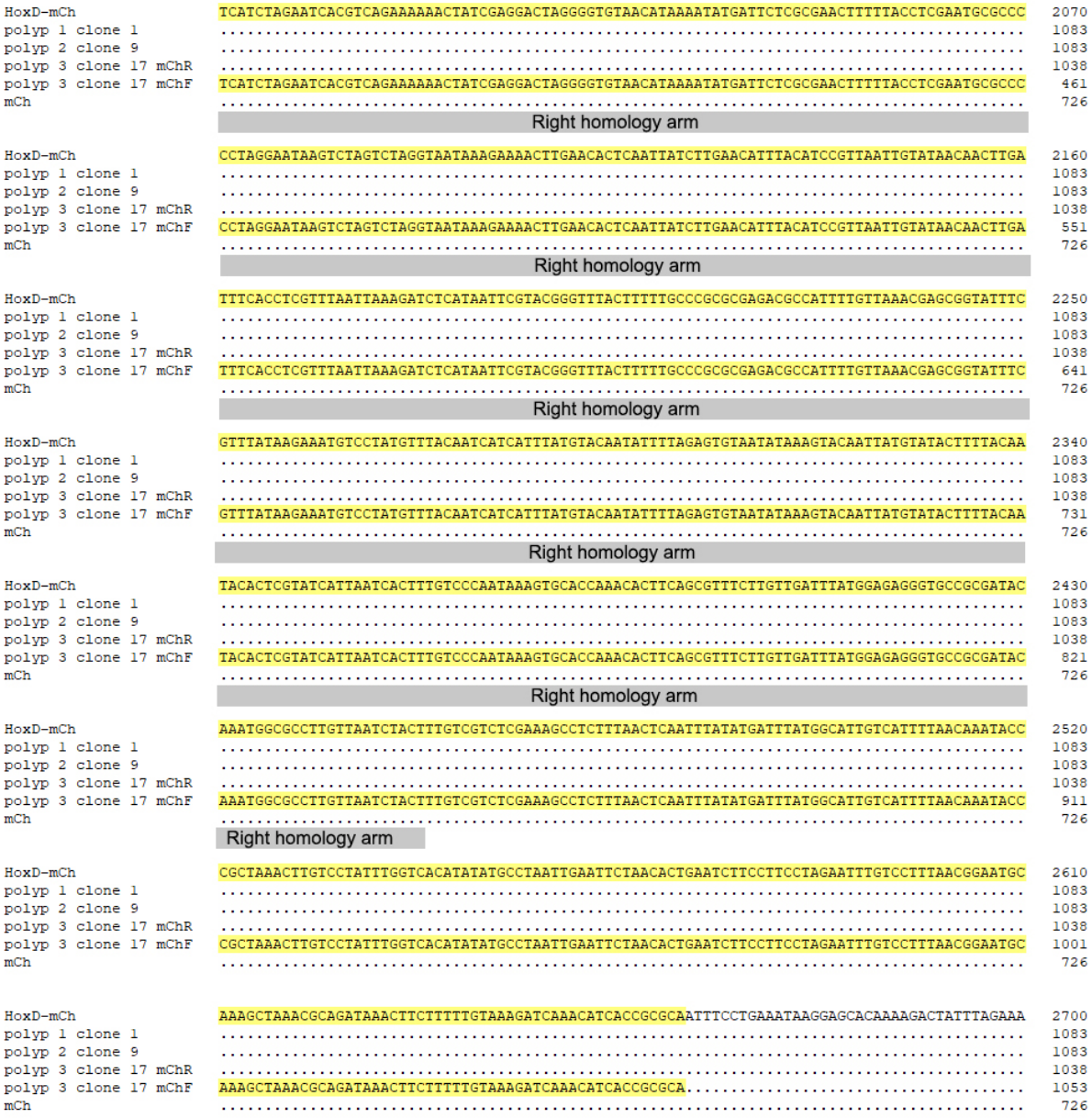

Fig. S8 Sequencing results of three *Nematostella* polyps confirming the knock-in of mCherry at the C-terminus of *HoxDa*.

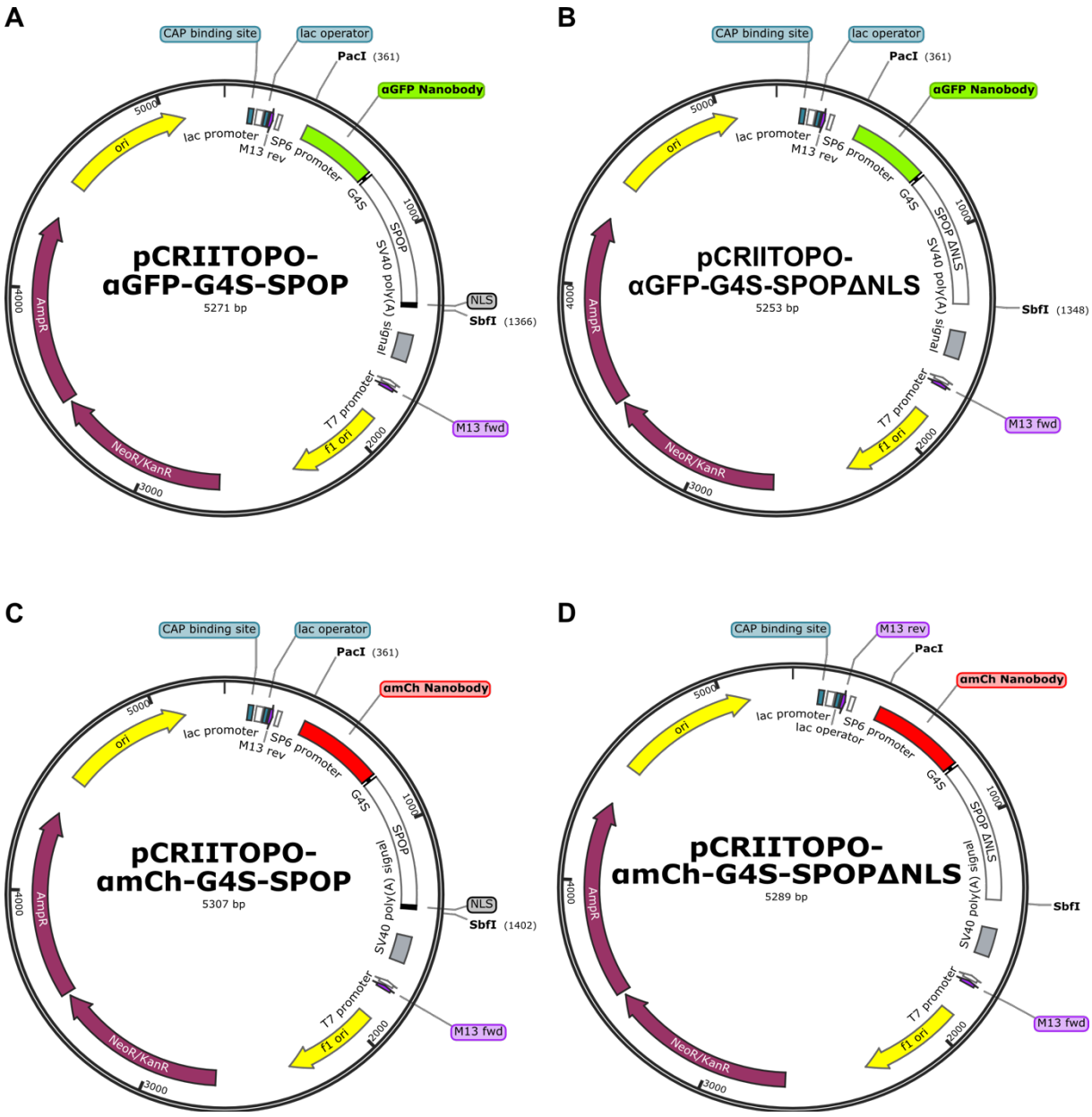

Fig. S9. Maps of plasmids used for in-vitro transcription of *Nb-SPOP* mRNA.

Table S1. crRNAs for *HoxDa, HoxB*, or *Gbx* with N- or C-terminal target sequences.

	Target gene	Target sequence	Genomic position
N-terminal	*HoxDa*/NVE21156	5′-CAGGTACCAGTATTGCACAG-3′	scaffold_61:675428
		5′-TTCGGTGTCAGTATTTTAGA-3′	scaffold_61:675501
	HoxB/NVE11345	5′-CGCTCCATCTCAGCAAGAAG-3′	scaffold_26:1276347
		5′-GGAACGCAGCGTGATGTGTA-3′	scaffold_26:1276265
	Gbx/NVE20684	5′-AATCAGAGATAGCTTCCGAT-3′	scaffold_58:1034228
		5′-TAGTAACAATTGACGCAACT-3′	scaffold_58:1034310
C Terminal	*HoxDa*/NVE21156	5′-TTGCAGACCGAATTTAACCG-3′	scaffold_61:677159
	HoxB/NVE11345	5′-ATGGTGGACAAAGATCAGTG-3′	scaffold_26:1273272
	Gbx/NVE20684	5′-TGGCTGGTACATCAATATAT-3′	scaffold_58:1035474

Table S2. Names and corresponding accession numbers of *Nematostella* and *Xenopus* Kelch-like proteins used for phylogenetic analysis. Orthologous proteins are marked in the same colour.

Nematostella		*Xenopus*	
Protein Name	**Accession Number**	**Protein Name**	**Accession Number**
Kelch-like-protein-2_1	NVE19530	Kelch-like-protein-2	XP-018098716.1
Kelch-like-protein-2_2	NVE863	Kelch-like-protein-4	XP-018085424.1
Kelch-like-protein-2_3	NVE17117	Kelch-like-protein-5	XP-018084635.1
Kelch-like-protein-3	NVE19807	Kelch-like-protein-6	XP-018121339.1
Kelch-like-protein-5	NVE8038	Kelch-like-protein-7	NP-001004916.1
Kelch-like-protein-8	NVE15434	Kelch-like-protein-8	NP-001017289.1
Kelch-like-protein-10	NVE17002	Kelch-like-protein-9	XP-018084922.1
Kelch-like-protein-12	NVE20403	Kelch-like-protein-10	XP-018096780.1
Kelch-like-protein-17_1	NVE10752	Kelch-like-protein-11	XP-002939078.1
Kelch-like-protein-17_2	NVE13095	Kelch-like-protein-12	XP-041437891.1
Kelch-like-protein-17_3	NVE21632	Kelch-like-protein-13	NP-001008095.1
Kelch-like-protein-17_4	NVE17833	elch-like-protein-14	XP-002934163.1
Kelch-like-protein-18_1	NVE2294	Kelch-like-protein-15	XP-041439530.1
Kelch-like-protein-18_2	NVE22294	Kelch-like-protein-17	XP-041425265.1
Kelch-like-protein-20_1	NVE21542	Kelch-like-protein-18	XP-018124455.1
Kelch-like-protein-20_2	NVE12129	Kelch-like-protein-20	NP-001086544.1
Kelch-like-protein-20_3	NVE3326	Kelch-like-protein-21	NP-001088480.1
Kelch-like-protein-20_4	NVE1117	Kelch-like-protein-22	XP-018099591.1
Kelch-like-protein-20_5	NVE16294	Kelch-like-protein-23	XP-018091378.1
Kelch-like-protein-20_6	NVE21179	Kelch-like-protein-24	XP-018121340.1
Kelch-like-protein-20_7	NVE4680	Kelch-like-protein-25	XP-018110799.1
Kelch-like-protein-20_8	NVE919	Kelch-like-protein-26	XP-041435882.1
Kelch-like-protein-28_1	NVE22694	Kelch-like-protein-28	XP-018085994.1
Kelch-like-protein-40	NVE10943	Kelch-like-protein-29	XP-041421002.1
		Kelch-like-protein-30	NP-001085193.1
		Kelch-like-protein-31	XP-018121044.1
		Kelch-like-protein-34	XP-018104036.1
		Kelch-like-protein-35	XP-018105898.1
		Kelch-like-protein-36	XP-041446124.1
		Kelch-like-protein-38	XP-018122837.2
		Kelch-like-protein-40	XP-018122558.1
		Kelch-like-protein-42	XP-018110367.1

Table S3. Primers used for synthesising the nanobody constructs.

Position	Name	Sequence 5´-3´
PacI-amCherry	Pac-amChnbF	TTAATTAAatggcacaggttcagctggt
amCherry-G4S-SPOP	mch-G4S-SPOPR	GAGCTTCCACCTCCACCtgtaaacgggctgctaa
amCherry-G4S-SPOP	SPOP_F	ttagcagcccgtttacaGGTGGAGGTGGAAGCTC
SPOPΔNLS-SbfI	SPOPNLS_SbfIR	CCTGCAGGCTAGCGTGGCGG
SPOP-SbfI	SPOP-SbfI	CCTGCAGGCTATGATGTCTT
PacI-aGFP	Pac-aGFPnbF	ttaattaaATGGATCAAGTCCAACTGGT
aGFP-G4S-SPOP	aGFPnb-G4S-SPOPR	GAGCCCGATACATTTACAGAGCTTCCACCTCCACCGCTGGAGACGGTGACCTG
SPOP	SPOP155F	TCTGTAAATGTATCGGGCTC
SPOPΔNLS-Sbf	Sbf-SPOP-NLS	cctgcaggCTAGCGTGGCGGGCCAATCATG
SPOP-Sbf	Sbf-SPOP_GR	cctgcaggCTATGATGTCTTTTGTCTCTTG

Table S4. Statistical analysis of the fluorescence intensity measurements

Group	Treatment	Test	Test Statistic (W/t)	p-value	Result
sfGFP-β-catenin	aGFP-SPOP	Shapiro-Wilk Normality	0.96378	0.001124	Non-Normal
	amCh-SPOP		0.99222	0.6803	Normal
	Uninjected		0.98967	0.302	Normal
	aGFP-SPOP vs amCh-SPOP	Mann-Whitney U test	0	< 2.2e-16	Significant
	aGFP-SPOP vs uninjected		1	< 2.2e-16	Significant
	amCh-SPOP vs uninjected	Welch Two Sample t-test	15.631	0.1191	Not significant
TBP::mCherry	aGFP-SPOP	Shapiro-Wilk Normality	0.9805	0.3096	Normal
	amCh-SPOP		0.98214	0.4386	Normal
	aGFP-SPOP vs amCh-SPOP	Welch Two Sample t-test	0.29536	0.7682	Not significant
mCH-SPOP + mCH mRNA 24hpf	aGFP-SPOP	Shapiro-Wilk Normality	0.91701	0.0006516	Non-Normal
	amCh-SPOP		0.90648	0.0002578	Non-Normal
	aGFP-SPOP vs amCh-SPOP	Mann-Whitney U test	2057	0.08898	Not Significant
mCH-SPOP + mCH mRNA 48hpf	aGFP-SPOP	Shapiro-Wilk Normality	0.97763	0.2432	Normal
	amCh-SPOP		0.99142	0.9441	Normal
	aGFP-SPOP vs amCh-SPOP	Welch Two Sample t-test	10,15	< 2.2e-16	Significant

Table S5 qPCR primers.

	GeneID	Name	Sequence 5´-3´
N-terminal	HoxDa/NVE21156	HoxDa_gF1	TGCACTTTAAGATAGCGAGGTCG
		HoxDa_gR1	CTCGCCTTCTCCGTACGTGTAT
	HoxB/NVE11345	HoxB_gF1	GGTTTGCGTTGTCATCGTGTT
		HoxB_gR1	TTGTTTCCTCTGGGATTCTCCA
	Gbx/NVE20684	Gbx_gF1	ATGACAACCGCAACTGCAAG
		Gbx_gR1	GGCGCATAGCAAGCAACTAAA
C-terminal	HoxDa/NVE21156	HoxD-meltF1	CCATTATCGTCGGCACTAGC
		HoxD-meltR1	GCACAATATGGCGTATGGAATC
	HoxB/NVE11345	HoxB-meltF1	ACTGCCTTCCAGCCTGTTAG
		HoxB-meltR1	TCAGTACTCTGGAGCAAATAAGGG
	Gbx/NVE20684	Gbx-meltF1	GCACATGGAAATGCCAAGAA
		Gbx-meltR1	AATCTCTGTCTTTCCCATTCCC

Table S6. 5'-Biotinylated primers used for synthesizing short homology arm HDR donor templates.

GeneID	Name	Sequence (5'Biotin-3´)
HoxDa	HoxD_mLHA-G2SmCh	CATTGTACATTCCAAACTCTCGGTCAGCGTGttTaCatTCaggaggtagtggcggttcaGTG
	HoxD_mRHA-mCh	GTTTTGAAAATAGTTAAATAAACCACAAATTTACTTGTACAGCTCGTCCA
HoxB	HoxB_LHA-G4S-GFP	CGGCTTTGGAGGCATTTCTATGCACAATGGcGGtCAgAGgTCtGTaTGagCTCAtTTtAGtGGTGGTGGTGGTAGTGTGAG
	HoxB_RHA-GFP	cattgCATATATATATATGTTTATGGAATCACTTGTACAGCTCGTCCATGC
GBX	GBX-LHA-G4SmCer	TTTGTGGCTATGAATCAAGCGAATGCTTTAGGTGGAGGTGGAAGCGTGAGCAAGGGCGAGGAGCT
	GBX-RHA_mCer	ACAAAATCTAAACGTAAACGGCAAAATGTTCTACTTGTACAGCTCGTCCA

Table S7. Plasmids containing reporter genes (and linker sequences) used for synthesising the HDR donor templates.

Name / CB-Number	Reporter	Used in HDR donor templates to	
CB258	mCherry	N-terminally tag	HoxD
CB246	GFP-G4S		HoxB
CB1775	mCerulean		Gbx
CB1707	G2SG2S - mCherry	C-terminally tag	HoxD
FGFalPr::BMPWTBFP	G4S-GFP		HoxB
CB1775	mCerulean		Gbx

Table S8. Sequencing primers for long homology arm HDR donor templates.

Name	Sequence 5´-3´	Sequenced region of donor template
ER 20	CTTCAAGGAGGACGGCAACATCCTG	Junction between RHA and GFP or mCerulean
ER 21	CAGGATGTTGCCGTCCTCCTTGAAG	Junction between LHA and GFP or mCerulean
ER 222	TTGGCGGTCTGGGTGCCCTCGTAG	Junction between LHA and mCherry
ER 223	CATCACCTCCCACAACGAGGACTACA	Junction between RHA and mCherry

Table S9. Primers used for genotyping suspected KI animals.

Gene - tag	Name	Sequence 5´-3´	Position
HoxD-mCH	HoxD_GT_F	agaaattccctgctcggtca	Upstream of LHA
	HoxD_GT_R	attgcgcggtgatgtttgat	Downstream of RHA
	ER 222	TTGGCGGTCTGGGTGCCCTCGTAG	Inside mCH insert
HoxB-GFP	HoxB_GT_F	actcactgtggcttgtactct	Upstream of LHA
	HoxB_GT_R	GCTGAACTTGTGGCCGTTTA	Inside GFP insert
Gbx-mCer	Gbx_GT_F	GGCGTCTGAGGAAAAGAGTG	Upstream of LHA
	Gbx_GT_R	GAACTTCAGGGTCAGCTTGC	Inside mCer insert